AOARD/AFRL Final Report on

High conductive BBL/Graphene nanocomposite system

Grant number FA23861014081

2011-09-02

Soo-Young Park

Kyungpook National University

Department of Polymer Science

Report Documentation Page

Form Approved
OMB No. 0704-0188

1. REPORT DATE	2. REPORT TYPE	3. DATES COVERED
13 OCT 2011	**Final**	**10-05-2010 to 10-06-2011**

4. TITLE AND SUBTITLE
High thermal conductive BBL/graphene nanocomposite system

5a. CONTRACT NUMBER
FA23861014081

5b. GRANT NUMBER

5c. PROGRAM ELEMENT NUMBER

6. AUTHOR(S)
Soo-Young Park

5d. PROJECT NUMBER

5e. TASK NUMBER

5f. WORK UNIT NUMBER

7. PERFORMING ORGANIZATION NAME(S) AND ADDRESS(ES)
Kyungpook National University,#1370 Sangyuk-Dong, Buk-gu,Daegu 702-701,Korea (South),NA,NA

8. PERFORMING ORGANIZATION REPORT NUMBER
N/A

9. SPONSORING/MONITORING AGENCY NAME(S) AND ADDRESS(ES)
AOARD, UNIT 45002, APO, AP, 96338-5002

10. SPONSOR/MONITOR'S ACRONYM(S)
AOARD

11. SPONSOR/MONITOR'S REPORT NUMBER(S)
AOARD-104081

12. DISTRIBUTION/AVAILABILITY STATEMENT
Approved for public release; distribution unlimited

13. SUPPLEMENTARY NOTES

14. ABSTRACT
Electrical conductivity of graphene/poly(benzimidazobenzophenanthroline) (BBL) composites was evaluated. Both graphene oxides (GOs) and reduced GOs (rGOs) were found to be well dispersed in BBL; in situ thermal reduction of GO was possible due to the high thermal degradation temperature of BBL (>600 C). Electrical conductivity of the GO/BBL composite increased by approximately 4 orders after annealing at 500 C for 30 minutes. Chemically-reduced GOs were also applicable to the rGO/BBL nanocomposite system and the post-heat treatment of the GO/BBL composite was also effective to impart good electrical conductivity to BBL.

15. SUBJECT TERMS
Polymer Matrix Composites, Graphene, thermal conductivity

16. SECURITY CLASSIFICATION OF:			17. LIMITATION OF ABSTRACT	18. NUMBER OF PAGES	19a. NAME OF RESPONSIBLE PERSON
a. REPORT	b. ABSTRACT	c. THIS PAGE			
unclassified	**unclassified**	**unclassified**	**Same as Report (SAR)**	**52**	

Figure List

of T_a and annealing time; the graphite oxide films were annealed under N_2 atmosphere.

Figure 14. The electrical conductivity vs. annealing temperature at different ϕs; the annealing was done for 30 minutes at N_2 atmosphere.

Figure 15. The TGA thermogram of the GO(20 wt%)/BBL composites before and after annealing at 400 °C.

Figure 16. (a) The fractured surfaces of the the GO(10 wt%)/BBL nanocomposite and (b) its two-dimensional wide angle X-ray pattern; the normal of the film surface is parallel to the horizontal direction; the white curved line was due to the shadow of the film .

Figure 17. The electrical conductivity vs. annealing temperature of the rGO_H(10 wt%)/BBL, rGO_{LAA}(10 wt%)/BBL, rGO_{NA}(10 wt%)/BBL, and rGO_{DMF}(10 wt%)/BBL.

Figure 18. The electrical conductivity of the rGO_H(10 wt%)/BBL, rGO_{LAA}(10 wt%)/BBL, rGO_{NA}(10 wt%)/BBL, and rGO_{DMF}(10 wt%)/BBL vs. O/C ratios of rGOs.

Summary: From this study, we found that the graphene oxides (GOs) and reduced GOs (rGOs) were well dispersed in BBL due to the interactions between delocalized π electrons in both poly(benzimidazobenzophenanthroline) (BBL) and the carbon sheets of the graphene so that the electrical-conductivity levels of the composites were proportional to those of their fillers of the rGOs; aggregations between the rGOs in BBL would cause the poor electrical conductivity and deviation from the linear relationship of the electrical conductivity between the filler and the composite. The thermal reduction after dispersing GOs in BBL was also possible due to the high thermal degradation temperature of BBL (> 600 °C); the electrical conductivity of the GO/BBL composite increased ~ 4 orders by annealing at 500 °C for 30 minutes. Thus, we found that the chemically-reduced GOs was applicable to the rGO/BBL nanocomposite system and the post-heat treatment of the GO/BBL composite was also effective to impart good electrical conductivity to BBL. Following are the details of our discovery in this study.

1) GOs were chemically reduced with hydrazine (rGO_h), $NaBH_4$ (rGO_{NA}), L-ascorbic acid (rGO_{LAA}), and DMF (rGO_{DMF}). Chemically (with $NaBH_4$) and thermally (at 1000 °C in N_2 gas) reduced GOs (rGO_{CT}s) were also prepared. The reduction levels of rGOs (examined with XPS, Raman spectroscopy, and FT-IR) were in the order of rGO_{CT}, rGO_h, rGO_{NA}, rGO_{LAA} and rGO_{DMF}. The oxygen/carbon (O/C) ratio of the rGO_{CT} (from the XPS spectrum) was 0.053 indicating that the oxygen-containing groups of the rGO_{CT} were almost removed. However, those of the rGO_h, rGO_{NA}, rGO_{LAA} and rGO_{DMF} were 0.104, 0.127, 0.168, and 0.179, respectively. The remaining oxygen-containing groups were beneficial to dispersion in organic solvents such as DMF, NMP, DMAc, etc. although a further reduction is necessary to get higher electrical conductivity.

2) The mechanism of the thermal reduction of the GO was also studied with X-ray

photoelectron spectroscopy (XPS), infrared spectroscopy (FT-IR), Raman spectroscopy, X-ray diffraction (XRD), and thermogravimetric analysis (TGA). The oxygen-containing groups were reduced step-wise at ~ 220 ^{o}C due to removal of the –OH and –COOH groups. These results suggest that the annealing at ~ 220 ^{o}C might recover partial electrical conductivity of the GO (from 10^{-6} to 13 S/cm within less than 10 min) and provide a methodology for developing an electrically conducting composite system by first dispersing the GOs in the matrix, then exfoliation by sonication, and finally heating the composite system at desirable temperatures although complete recovery of the electrical conductivity may not be possible with moderate heat treatment.

3) The BBL/graphene nanocomposites were prepared with a solution blending in methanesulfonic acid (MSA) with GO, rGO_h, rGO_{NA}, rGO_{LAA}, rGO_{DMF}, and rGO_{CT}. The GOs as well as the rGOs were well dispersed in BBL due to the interactions between the delocalized π electrons in both the BBL and the graphene-carbon sheet. The electrical conductivity of the rGO_{CT} (10 wt%)/BBL was ~ 0.0023 S/cm, and those of the rGO_h(10 wt%)/BBL, rGO_{LAA}(10 wt%)/BBL, rGO_{NA}(10 wt%)/BBL, and rGO_{DMF}(10 wt%)/BBL were 0.0003, 0.0003, 0.0003, 0.0002 S/cm, respectively. The electrical conductivity of the rGO_{CT} (10 wt%)/BBL is approximately one order higher than those of the other rGO/BBLs because the additional thermal reduction of the already chemically-reduced GOs by $NaBH_4$ was conducted.

4) The GOs were thermally reduced in the GO/BBL nanocomposites. The electrical conductivities of the GO/BBLs proportionally increased as the amount of the GO (ϕ) increased although those were low in the range of 10^{-6} to 10^{-3} S/cm for ϕ = 10 to 90 wt%. The conductivities of GO/BBLs continuously increased as the annealing temperature increased. The conductivity levels of the annealed GO/BBLs increased ~ 4 orders by

annealing at 500 °C for 30 minutes due to thermal reduction of the GOs in the BBL matrix.

1. Introduction.

1-1. Gaphene: Graphene is a two-dimensional (2-D) single layer of sp^2-bonded carbons with one atomic layer thickness (Figure 1a).[1-3] It has recently attracted increasing attention because of its peculiar electronic properties such as quantum Hall effect,[4] 2-D Dirac fermions,[1a] an ambipolar electric field effect along with ballistic conduction of charge carriers,[1b] tunable band gap,[5] its extraordinary electrical, thermal, and mechanical properties that rival in-plane values of graphite,[1c,2,6] and its various promising potential applications such as composites,[1c,7] transparent conductive films,[8,9] lithium-ion batteries,[10] supercapacitors,[11] organic photovoltaic cells,[12,13] electron field emitters,[14] field effect transistors,[15] and ultrasensitive sensors.[16] **Their thermal conductivity and mechanical stiffness may rival the remarkable in-plane values for graphite (~5,300 $Wm^{-1}K^{-1}$ and ~1 TPa, respectively), their fracture strength should be comparable to that of CNTs for similar types of defects (see Table 1)**.[17-19]

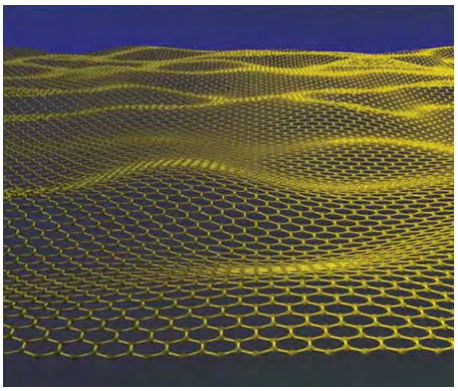

(a)

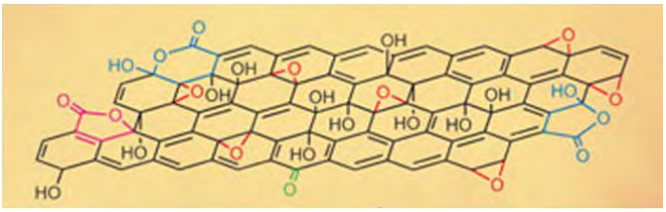

(b)

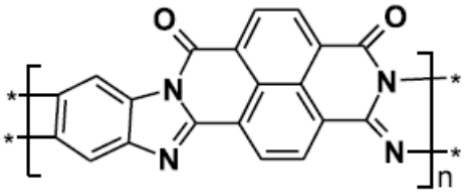

(c)

Figure 1. (a) Graphene, (b) GO, and (c) BBL chemical structures.

Table 1. Physical properties of SWNT and graphene[20]

Property	Single-walled CNTs	Graphene
Specific gravity	0.8 g/cm^3	1.8–2.2 g/cm^3
Elastic modulus	~1 TPa (axial direction)	~1 TPa (in-plane)
Strength	50–500 GPa	~100–400 GPa
Resistivity	5–50 μΩ cm	50 μΩ cm (in-plane)
Thermal conductivity	Up to 2,900 Wm^{-1} K^{-1} (estimated)	5,300 Wm^{-1} K^{-1} (in-plane) 6–30 Wm^{-1} K^{-1} (*c*-axis)
Magnetic susceptibility	22 × 10^6 emu/g (radial) 0.5 × 10^6 emu/g (axial)	22 × 10^6 emu/g (⊥ to plane); 0.5 × 10^6 emu/g (∥ to plane)
Thermal expansion	Negligible in the axial direction	−1 × 10^{-6} K^{-1} (in-plane) 29 × 10^{-6} K^{-1} (*c*-axis)
Thermal stability	>700 °C (in air); 2800 °C (in vacuum)	450–650 °C (in air)
Specific surface area	Typically 10–200 m^2/g Up to 1,300 m^2/g	Typically 100–1,000 m^2/g, up to >2,600) m^2/g

These data were obtained from various open-literature sources.

1-2. Graphene/polymer nanocomposite: One possible route to harnessing graphene's

exceptional properties for applications would be to incorporate graphene sheets in a matrix material as a second-phase filler to substantially enhance the electric, thermal, and mechanical properties. Composite materials employing carbon-based materials such as carbon-nanotube (CNT), graphene, and fullerene have been explored. However, at present, CNTs have dominated carbon-based nanocomposite as the choice of a filler although the intrinsic bundling of CNTs, the impurities from the catalysts, and high costs have been hampering their application. Graphene/polymer nanocomposites have not relatively been studied compared to CNT/polymer nanocomposites although the properties of the graphene are comparable to those of CNT or superior in some properties such as thermal conductivity. It was recently reported that a polystyrene/graphene nanocomposite exhibits a percolation threshold in electric conductivity at filler volume fraction as low as 0.1 vol %, comparable to those observed in carbon nanotube-based composites[1c] and a conductivity of 0.1 Sm^{-1}, sufficient for many electrical applications.[21] The manufacturing of such composites requires not only that graphene sheets be produced on a sufficient scale but that they also be incorporated, and homogeneously distributed, into various matrices. Thus, the preparation of the graphene/polymer composites *via* complete exfoliation of graphite[22] and molecular-level dispersion of chemically modified graphene sheets within polymer hosts are essential for maintaining the novel properties of the graphene in the nanocomposite. Several strategies have been developed to produce this completely exfoliated 2-D carbon material, such as mechanical cleavage,[1b] epitaxial growth on SiC[23] or metal substrates,[24] and chemical exfoliation of graphite.[25-27] Among these methods, **chemical exfoliation is widely considered as a promising approach for large-scale production of graphene sheets which can be made from graphite which is inexpensive and available in large quantity**.

1-3. Graphene Oxide (GO): Perfect graphene itself does not occur naturally, but bulk and solution-processable functionalized graphene can be prepared through extensive chemical attack of graphite crystals to introduce oxygen-containing defects in the graphite stack followed by complete exfoliation into sheets of atomic-thickness through either thermal or mechanical treatments.[28] This oxygenated graphite is called as graphene oxide (GO) (Figure 1b). GO sheets are composed of planar, graphene-like aromatic domains of random sizes interconnected by a network of cyclohexane-like units in chair configuration which are decorated by hydroxy, epoxy, ether, diol, and ketone groups.[29] The presence of these functional groups makes graphene oxide sheets strongly hydrophilic, which allows GO to readily swell and disperse in water.[18,30,31] A mild ultrasonic treatment of GO in water results in its exfoliation to form stable aqueous dispersions that consist almost entirely of 1-nm-thick sheets.[22] The dispersion behavior of GO in different organic solvents, such as DMF, NMP, ethylene glycol and THF has been studied.[32] The GOs have recently attracted attention as a choice of a filler for polymer nanocomposites due to its solution-process ability.[33-,35]

However, the GOs suffer from poor quality mainly because of the introduction of oxygen-containing functional groups during synthetic process, which consequently prevents their further applications, especially as electrically conductive composites and nanodevices. As a result, **a post-treatment process, such as reduction of GOs by chemical method**[25,27,36] **or thermal annealing,**[9,37] **is required to remove the oxygen-containing groups after the material has been processed into the final form.**[25] Chemical reduction of exfoliated GO by reducing agents, such as hydrazine and dimethylhydrazine appears to be a promising strategy for the large-scale production of graphene.[1c,38] Refluxing GO in hydrazine or treating graphene oxide with hydrazine in a microwave oven ensures reduction. **But reduction of the exfoliated GO nanoplatelets in solution results in their irreversible coagulation,**[22]

which then makes dispersion within a polymer matrix at the individual sheet level impossible.

1-4. Thermal conduction: A high temperature annealing method is also effective in deoxygenating the films and restoring conductivity.[9,37] XPS measurements showed that the percentage of oxygen-containing functional groups was dramatically decreased during heating, and the ratio of C/O of the final material was close to those of the chemically reduced GOs,[25] indicating that the exfoliation and partial deoxygenation of GO can be realized during the heating process. Similar thermal processes have been successfully used to remove oxygen-containing functional groups from carbon nanotubes[39] and to fabricate transparent electrodes from thin photo-resist films.[40] Aksay and co-workers proposed a thermal exfoliation method for the production of graphenes in a large quantity, where a rapid heating process was involved to exfoliate GO by quickly moving the GO into a furnace preheated to a high temperature.[41,42] The reported conductivities were in the order of 10^2 S/cm (R_s< 1 kΩ/square) with greater than 80 % light transmittance in the 400–1800 nm wavelength range suggesting that the reduction of the GOs could be achieved by a thermal annealing method. GOs can be easily dispersed in polymer the matrix material and heat treatment of the GO/polymer nanocomposite could recover good properties of the graphene in the nanocomposite. **In order to apply thermal reduction to the GO/polymer nanocomposite, the matrix should be stable at high temperatures.** In this proposal, BBL, is proposed for a matrix material in the graphene/polymer nanocomposite because of high thermal stability as well as other novel properties.

1-5. BBL(poly(benzamidazobenzophenanthroline))**:** The fully conjugated ladder polymer,

BBL has a repeat unit that possesses a double-stranded chemical structure consisting of aromatic napthalenic and benzenoid units and alternating bond lengths of imines in the neutral ground state (Figure 1c). BBL has novel properties such as high thermal and thermo-oxidative stabilities, exceptional resistance to organic solvents, good mechanical properties as fibers and films, interesting opto-electronic properties due to its structural and molecular order, dramatically enhanced thermally induced electronic conductivity,[43-,45] n-type (electron transport) organic semi-conductor based on electrochemical doping experiments,[46-,49] photo-induced electron transfer and photoconductivity,[50-,53] and NLO property with large third-order optical non-linearities.[54] These BBL properties have been evaluated for potential utilization in many opto-electronic devices that include p-n junctions, organic thin film transistors, light emitters, tunable electrochromic and electroluminescent devices, polymer-based light sensors, xerographic imaging systems, and photovoltaic (solar) cells.[55-61] **BBL is first synthesized[62] as a structural material for its anticipated high tensile strength, and provides a model system because of its stability at temperatures up to 600 °C in air and 700 °C in nitrogen and the processability by which thin films and fibers of micron-size diameter can be obtained.**[63] These polymers, in the form of films or fibers, due to their high molecular weight, display good mechanical properties (high tensile strength, high modulus) and exceptional solvent chemical resistance.[64] BBL has received interest as a conductive[65] and nonlinear optical[66] material due to its electronic conjugation and their **extensive π electron delocalization**, coupled with high mechanical strength, and thermal stability.[63]

Conjugated polymers such as polyacetylene, polythiophene and polyaniline have been widely studied for electronic and electro-optical properties.[67] These polymers are insulators in pristine state and show metallic conductivity in the oxidized or reduced state. The highest conductivity was found for the highly stretched and heavily doped systems.

Problems encountered for practical applications of these conjugated polymers are intractability, environmental instability, and degradation upon doping, in various degrees. BBL belongs to a different class of conjugated polymers which are thermally and environmentally stable due to their aromatic structures. However, there are far fewer studies on the electronic transport of BBL compared to the conventional conducting polymers such as polyacetylene, polyaniline, polypyrole, etc.[68] Another aspect that has not been studied in conventional conducting polymers, primarily due to lack of thermal stability, is the behavior of electronic properties in the high-temperature ~230 to 430 ^{o}C regime at which BBL is quite stable.

BBL has been studied for improved electrical conductivity by chemical doping,[69] ion implantation, pyrolysis, and heat treatment.[70] Pristine BBL is a semiconductor with a room temperature conductivity of 3 X 10^{-10} S/cm.[71] Electrochemically doped samples show conductivities as high as 20 S/cm.[72] **Heat treatment of BBL at 100 to 350^{o}C dramatically and reversibly increases the room temperature dc conductivity,[73] reaching a maximum conductivity of about 3 X 10^{-4} S/cm for the 350^{o}C treatment.**

1-6. BBL/graphene nanocomposite: The BBL/graphene nanocomposite might be a good combination for a high performance composite system because GO can be easily dispersed in MSA and poly(phosphoric acid) (PPA) which are good solvent and polymerization medium, respectively. **This BBL/GO nanocomposite can be heat-treated for reduction of GO to graphene in the BBL matrix. BBL is also stable up to ~700 ^{o}C in nitrogen and can increase the electrical conductivity by heat treatment. Thus, the exceptional electrical properties can be generated in BBL/graphene nanocomposite system.** One of the applications of the BBL/graphene nanocomposite might be electromagnetic interference

(EMI) shielding. Because of the wide use of commercial, military and scientific electronic devices and communication instruments, EMI shielding of radio frequency radiation continues to be a serious concern for modern society. Compared with conventional metal-based EMI shielding materials, conducting polymer composites are lightweight, resistant to corrosion, and flexible and offer processing advantages[74]. The EMI shielding effectiveness (SE) of a composite material mainly depends on the filler's intrinsic conductivity, dielectric constant and aspect ratio. Thus, it is expected that the use of atomic thick graphene, with large aspect ratio and high conductivity, would provide a high EMI SE. In particular, BBL/graphene nanocomposite can survive at the harsh conditions so that it might be suitable for aerospace materials.

1.7. What we did in this work:

1) **Reduction of the GOs**: the GOs were chemically reduced with hydrazine (rGO_H), $NaBH_4$ (rGO_{NA}), L-ascorbic acid (rGO_{LAA}), and DMF (rGO_{DMF}). Chemically (with $NaBH_4$) and thermally (at 1000 °C in N_2 gas) reduced GOs (rGO_{CT}s) were also prepared. The degrees of reductions of rGOs were examined with XPS, Raman spectroscopy, and FT-IR.

2) **The mechanism of the thermal reduction of the GO**: The GOs were annealed at different temperatures up to 1000 °C. Their mechanisms were also studied with XPS, FT-IR, Raman spectroscopy, X-ray diffraction, and thermogravimetric analysis (TGA).

3) **Preparation of the BBL/graphene nanocomposites**: The BBL/graphene nanocomposites were prepared with a solution blending in methanesulfonic acid (MSA) with GO, rGO_H, rGO_{NA}, rGO_{LAA}, rGO_{DMF}, and rGO_{CT}. The conductivity and their structures were studied in this work

4) **Thermal reduction of the GO in the GO/BBL composite**: The GOs were thermally

reduced in the GO/BBL, and their conductivities were compared with the chemically reduced composites.

2. Experimental

2-1. GO preparation: The graphite used in this study was purchased from Samjung C&G Inc.© (FP 99.95). The GO was synthesized by using the modified Hummers method. A small amount of flake graphite (4g) was vigorously stirred for 3 hours in a concentrated H_2SO_4 (92ml) solution of $NaNO_3$ (2g) and $KMnO_4$ (12g), washed with a 5 wt% aqueous H_2SO_4 solution, and treated with a 30 wt% aqueous H_2O_2 solution to reduce the residual permanganate and MnO_2 to colorless soluble $MnSO_4$ salts. The GO suspensions were filtered with filter papers and rinsed with distilled water more than 15 times until pH=7 was obtained. The GO powder was obtained after drying it at 60 ^oC in an oven. The GO film was made from the aqueous GO suspension. 20 mL of the GO powder (4mg/mL) were sonicated with a tip-type sonicator (Vibracell, VCX-750) for 1 hour and then heated at 60 ^oC in a Teflon-coated Petri dish. After drying completely, the deposited GO film was peeled off from the bottom of the glass. The resultant GO film was ~30 μm thick.

2-2. BBL: BBL (purchased from Alrich) has a molecular weight of 10113.

2-3. Chemical reductions:

2-3-1. rGO_{DMF}[75]: The rGO_{DMF}s were obtained by a simple one-step reduction approach. In a typical experiment, the as-synthesized GO was firstly dispersed in DMF (0.5 mg/mL) under ultrasonically treatment for 30 min, and then heated in an oil bath (153 °C) for 1 hour. DMF is widely used in the chemical industry due to its cost-effectiveness and high solvent power.

Moreover, DMF is a much better solvent and can be used as the source of carbon monoxide and dimethylamine originating from its decomposition at boiling point (153 °C). It is well known that carbon monoxide is a strong reducing agent, which could highly efficiently remove oxygen from many compounds and DMF molecules were efficient stabilizers of graphene sheets. Therefore, it is expected that graphite oxides can be reduced by endogenous reducing agent (CO) from DMF heated at its boiling point to produce soluble rGO_{DMF} sheets in large quantities (Figure 2). It is worth pointing out that rGO_{DMF}s could be easily dispersed in other solvents such as N-methyl-2-pyrrolidone (NMP), DMF, and dimethyl acetamide (DMAc) (Figure 2). Such high solubility of the rGO_{DMF} in various solvents was attributed to the stabilization of DMF absorbing on the graphene planes, since DMF is miscible with water and the majority of organic solvents.

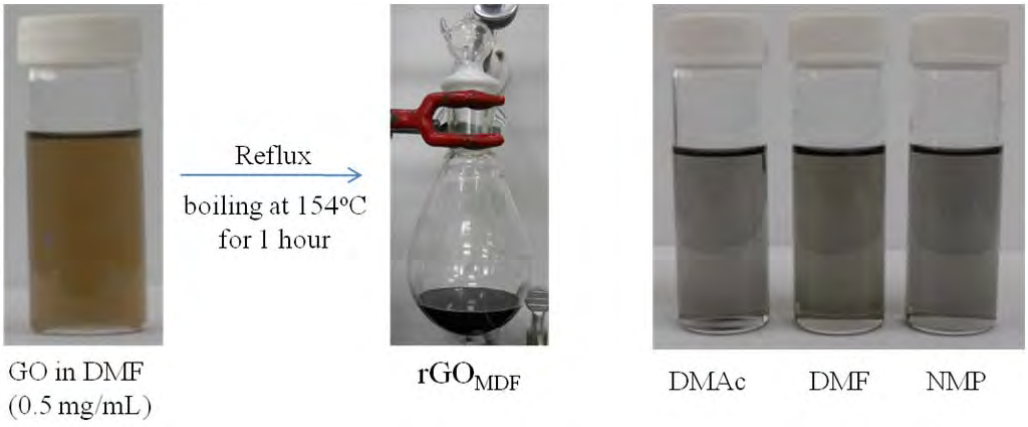

Figure 2. (Left) A digital image of GO in DMF before and after reduction, (right) the dispersion of rGO_{DMF} (0.1 mg/mL) in DMAc, DMF and NMP.

2-3-2. rGO_{LAA}[76]: L-Ascorbic acid (LAA), having a mild reductive ability and nontoxic property, is naturally employed as a reducing agent in living things, and has also been used as a primary reductant in the laboratory. Herein, we used a facile approach for reducing GO

sheets using LAA as a reductant in an aqueous solution at room temperature. Besides the pronounced reduction capability to GO, the oxidized products of LAA may also play a role as a capping reagent to stabilize as-reduced GO sheets simultaneously, avoiding the usage of additional capping reagents. More significantly, in comparison with the conventional reductants used in GO reduction, such as hydrazine and hydrazine hydrate, LAA itself and the oxidized products are environmentally friendly. The reduction of the GO using LAA was performed in water at room temperature (~23 °C). In a typical experiment, 50 mg of LAA was added to 50 mL (0.1 mg/mL) of an aqueous dispersion of the GO under vigorous stirring. After reduction, the color of the solution changed from gray to black as shown in Figure 3.

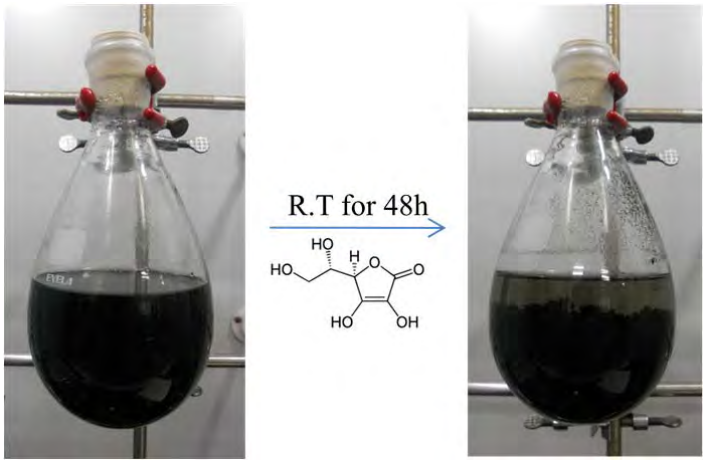

Figure 3. A digital image of reduction of GO with L-Ascorbic acid.

2-3-3. rGO_{CT}[77]: Figure 4 shows schematic representation of the $_rGO_{CT}$ reduction procedure. Dry GOs were dispersed in deionized water to give a 1mg/mL colloidal solution. The pH of this solution was adjusted to 9 ~ 10 by 5 wt% sodium carbonate solution. Sodium borohydride (800 mg, reagent grade, 98.5%, Sigma-Aldrich) was directly added into 100 ml GO dispersion under magnetic stirring, and the mixture was kept at 80 °C for 1 h with

constant stirring. The reduction product was separated by filtration and washed with large amounts of water several times to remove most residual ions. This partially reduced GO was kept in a vacuum desiccator with phosphorous pentoxide for two days and redispersed in concentrated sulfuric acid (UN 1830, reagent grade, Fisher Scientific) and heated to 120 °C with stirring for 12 hours. After cooling down, the dispersion was diluted with deionized water. The final product was separated by filtration and thoroughly rinsed with water to remove most impurities. The product powder was compressed into a pellet and further annealed at 1,000 °C under 1.3 standard liter per minute gas flow of N_2 for 15 minutes.

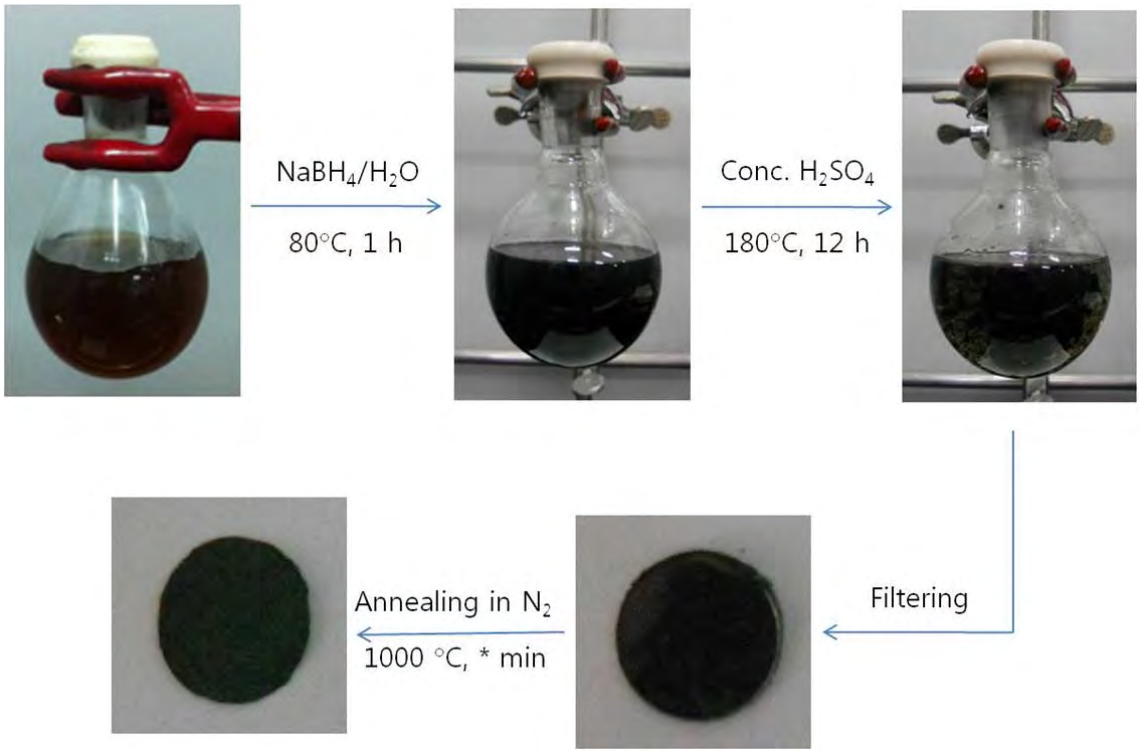

Figure 4. Schematic representation of the $_rGO_{CT}$ reduction procedure.

2-3-4. rGO_H[78]: Figure 5 shows the schematic of the rGO_H reduction procedure. The aqueous GO solution (100 mL, 1 mg/mL) was heated to 100 °C and then $N_2H_4.H_2O$ (1.00mL) was added in the aqueous GO solution for 12 hours. The color of the GO solution changed

from grey to black during reduction as shown in Figure 5. The solution was filtered with a paper filter (7µm) with an aspirator. The powder was dried in the vacuum oven for 12 hours. The dried powders were kept for further use.

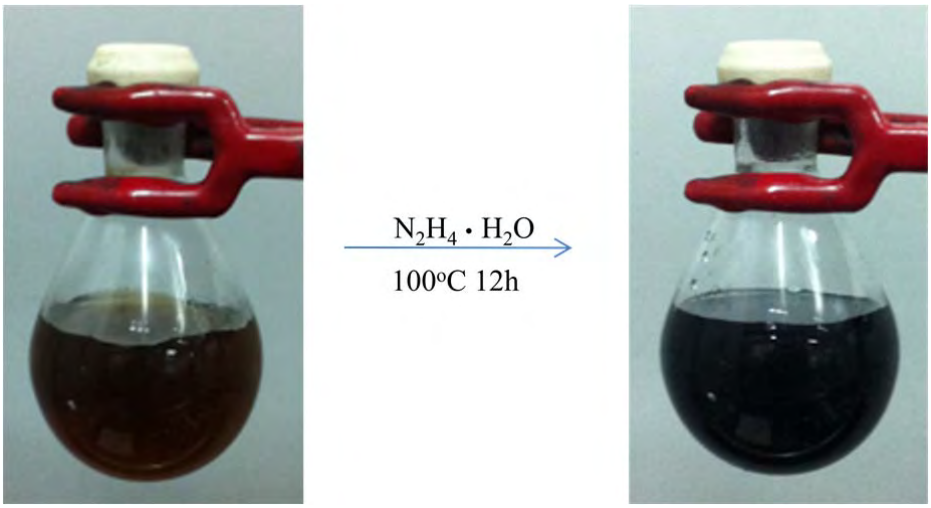

Figure 5. Schematic representation of the $_rGO_H$ reduction procedure.

2-3-5. rGO_{NA}[79]: Figure 6 shows the schematic of the rGO_{NA} reduction procedure. Typically, 120 ml GO suspension (2 mg/ml) was dispersed in 200 ml N, N -dimethylformamide (DMF) by ultrasonication, and 3 g $NaBH_4$ and 0.2 g anhydrous $AlCl_3$ were dissolved in 120 and 80 ml DMF, respectively. The above three kinds of solutions were mixed together and heated at 30 – 150 ^oC for 3 h. The solution was filtered with a paper filter (7µm) with an aspirator. The powder was dried in the vacuum oven for 12 hours. The dried powders were kept for further use.

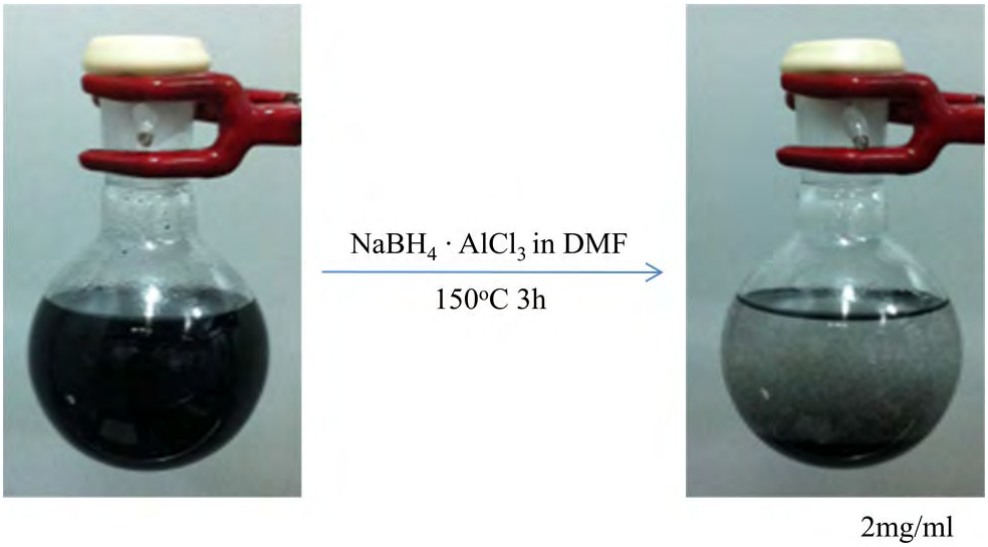

Figure 6. Schematic representation of the $_rGO_{NA}$ reduction procedure.

2-4. Film casting: The GO powders in MSA (1.5 mg/mL) were dispersed with a sonicator for 2 hours at 60 Hz, and the predetermined amount of BBL was dissolved and mixed with a magnetic stirring bar for 5 hours in the GO/MSA solution. The red viscous dope was poured on the glass plate and cast into a film by drawing a glass bar over the plate. The gap between the glass bar and the plate was controlled by thickness of the rolled tape on both end-edges of the glass bar. The film was immersed into a TEA/ethanol bath for a day to remove MSA and then dried in a sample holder. The amounts of the GO in the BBL were 10 to 90 wt% with 10 wt% intervals, the film thickness was ~ 20 μm, and the color of the films was gold.

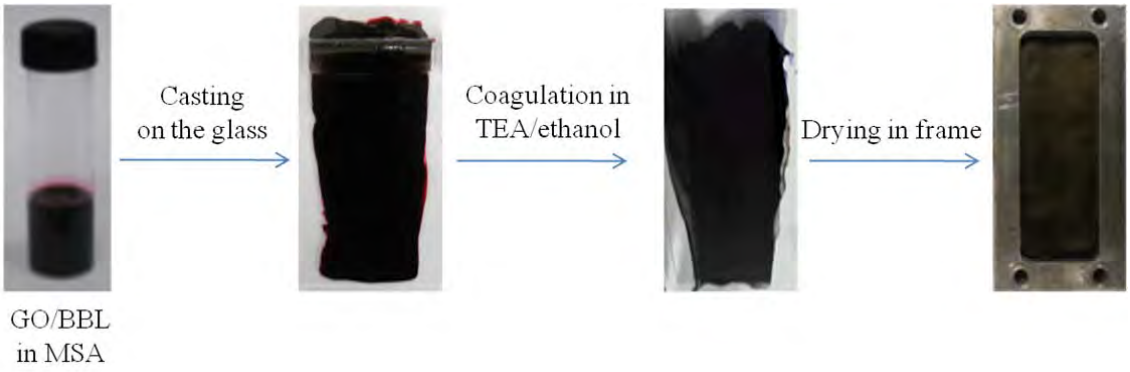

Figure 7. The scheme for the film preparation of the GO/BBL nanocomposite film.

2-5. Characterization:

2-5-1. SEM: Micrographs of the osmium tetroxide (OsO_4)-coated surface of the fractured GO/cellulose composite films in liquid nitrogen were taken using a Hitachi S-4800 scanning electron microscope (SEM) with an accelerating voltage of 15 kV.

2-5-2. TGA: Thermo gravimetric analysis (TGA) thermo grams of the composite were taken in a TGA-50 (Shimadzu co.) with a temperature range of 150 to 500 ^{o}C under a nitrogen atmosphere with a scan rate of 10 ^{o}C/min.

2-5-3. Electrical conductivity: The conductivities of the GO/cellulose composite films were measured at an ambient temperature by a four-point probe method using an HMS-3000 (Ecopia). The dimensions of the samples were about 10 (length) × 10 (width) × ~ 0.025 (thickness) mm^3 and their ends were coated with an indium paste to ensure good electrical contact. The instrumental limit of the electrical conductivity is in the range of 10^3 to 10^{-6} S/cm.

2-5-4. Wide angle X-ray scattering: Wide-angle X-ray diffraction patterns were recorded on a phosphor image plate (Perkin Elmer, Cyclone) by a Statton camera. An Anton-Parr X-ray generator, operated at 40 kV and 50 mA, produced Cu-K_α radiation, which was

monochromatized with a flat monochromator (Huber model 151). The sample-to-film distance was calibrated by SiO_2 powders.

2-5-5. FT-IR: FT-IR spectra of the GO and graphite powders were taken with an FT-IR spectrometer (FT/IR-620, Jasco co., Japan) under vacuum. The samples were vacuum-dried for 1 day, mixed with KBr, and pressed into a 13-mm diameter pellet. The spectra were derived from 50 co-added interferograms, which were obtained at a resolution of 1 cm^{-1}.

2-5-6. XPS: XPS measurements were performed on a VG Microtech ESCA 2000 using a monochromic Al X-ray source.

2-5-7. Raman spectroscopy: Raman spectra were taken on the samples on a Renishaw invia + Reflex spectrometer with an argon-ion laser at an excitation wavelength of 514.5 nm.

3. Results and discussion

3-1. Chemical reductions

3-1-1. XPS of rGOs: Figure 8 shows the XPS survey spectra of GO, rGO_{CT}, rGO_{H}, rGO_{LAA}, rGO_{NA}, and rGO_{DMF}. Graphitic C 1s and O 1s were observed at 284.7 and 531 eV, respectively. The peak of O 1s is higher than that of the C 1s in the case of GO. The O 1s peak was significantly reduced by reduction. The O/C ratios are 0.053, 0.104, 0.127, 0.168, 0.179, 0.463, for rGO_{CT}, rGO_{H}, rGO_{NA}, rGO_{LAA}, rGO_{DMF}, and GO, respectively as shown in Table 2. The O/C ratio of the rGO_{CT} is highest and decreased from 0.463 to 0.053 by reduction of the GO indicating that nearly all oxygen-containing groups were removed although the O/C ratios of other rGOs are in the range of 0.1 to 0.2. The nitrogen atom peak could not be found in the XPS spectrum of the rGO_{CT} which indicates that the doping with nitrogen atoms during thermal reduction in N_2 atmosphere was not observed**.** The O/C

ratios are in the order of rGO_{CT}, rGO_{H}, $rGO_{NA,}$ rGO_{LAA}, and rGO_{DMF}. The reductions with hydrazine and $NaBH_4$ were more effective in removing the oxygen-containing functional groups and the reductions with LAA and DMF were less effective than those with hydrazine and $NaBH_4$. However, rGO_{LAA}, and rGO_{DMF} were more dispersible in organic solvents.

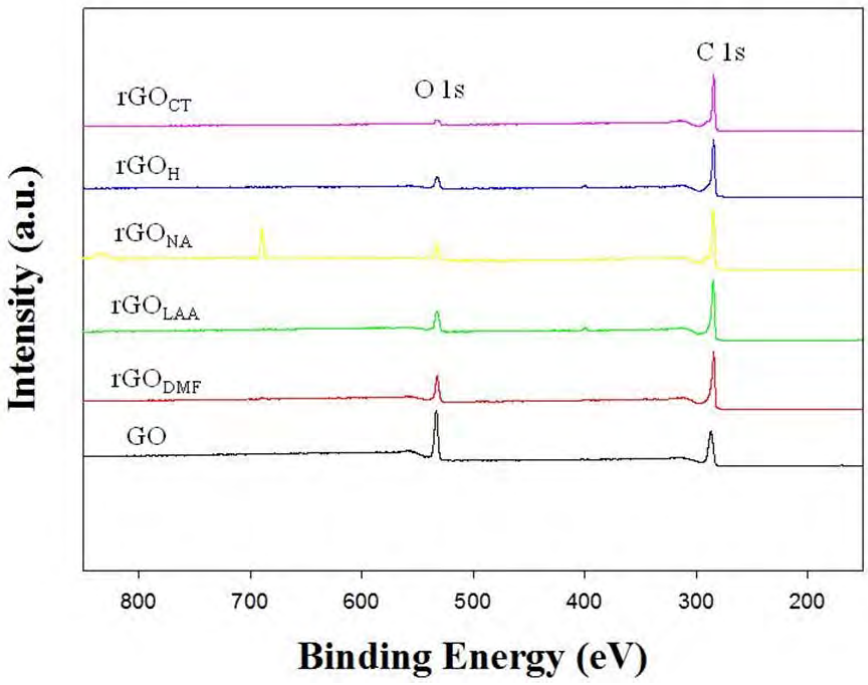

Figure 8. The XPS survey spectra of the rGO_{CT}, rGO_{H}, rGO_{LAA}, rGO_{NA}, and rGO_{DMF}

Table 2. The O/C ratios and electrical conductivities of rGO_{CT}, rGO_{H}, rGO_{LAA}, rGO_{NA}, and rGO_{DMF}

	O/C ratio	**Conductivity (S/cm)**	
		before annealing	**after annealing at 300°C**
rGO_{CT}	0.053	$2.340e^{-3}$	$4.210e^{-3}$
rGO_{H}	0.104	$3.044e^{-4}$	$2.888e^{-3}$

rGO_{NA}	0.127	$2.934e^{-4}$	$2.648e^{-3}$
rGO_{LAA}	0.168	$2.836e^{-4}$	$2.440e^{-3}$
rGO_{DMF}	0.179	$1.532e^{-4}$	$1.412e^{-3}$
GO	0.463	$6.897e^{-6}$	$1.423e^{-3}$

3-1-2. Raman spectroscopy of rGOs: Figure 9 shows the Raman spectra and their I(D)/I(G) ratios of the rGO_{CT}, rGO_{H}, rGO_{LAA}, rGO_{NA}, GO, graphite, and rGO_{DMF}. The two prominent peaks at ~1350 and ~ 1600 cm^{-1} correspond to the D and G bands, respectively. The peak positions of G bands of rGO_{DMF} and rGO_{LAA} are 1600 cm^{-1}. These are close to that of GO (1600 cm^{-1}), but higher than that of graphite (1580 cm^{-1}) (blue-shifted). However, the peak positions of G bands of the rGO_{CT}, rGO_{H}, and rGO_{NA} are 1580 cm^{-1}, close to that of graphite (1580 cm^{-1}). The peak positions of the D bands were relatively constant as compared to those of the G bands although the peaks of the rGO_{DMF} and rGO_{LAA} are broader than those of rGO_{CT}, rGO_{H}, and $rGO_{NA.}$ The blue shift of GO, rGO_{DMF} and rGO_{LAA} as compared to the graphite has been known to be due to the presence of single-double carbon bonds within the sp^2 carbon ribbons. To obtain these single-double bonds, it is necessary to have sp^3 carbons on the edges of a zigzag carbon ribbon by partial reduction.[80] The blue-shift decreased as more reduction occurred in rGO_{CT}, rGO_{H}, and rGO_{NA}. The I(D)/I(G) ratio is in the order of rGO_{CT}, rGO_{H}, rGO_{NA}, rGO_{LAA}, and rGO_{DMF}. The increase in I(D)/I(G) ratio is known to be a result of the formation of numerous small sp^2 domains upon reduction. The mechanism underlying the change in I(D)/I(G) ratio due to functionalization, however, remains unclear so far. However, the order of I(D)/I(G) ratio is the same as those of the O/C ratio and the electrical conductivity, indicating that the degree (the perfectness) of the reduction is strongly related to the I(D)/I(G) ratio.

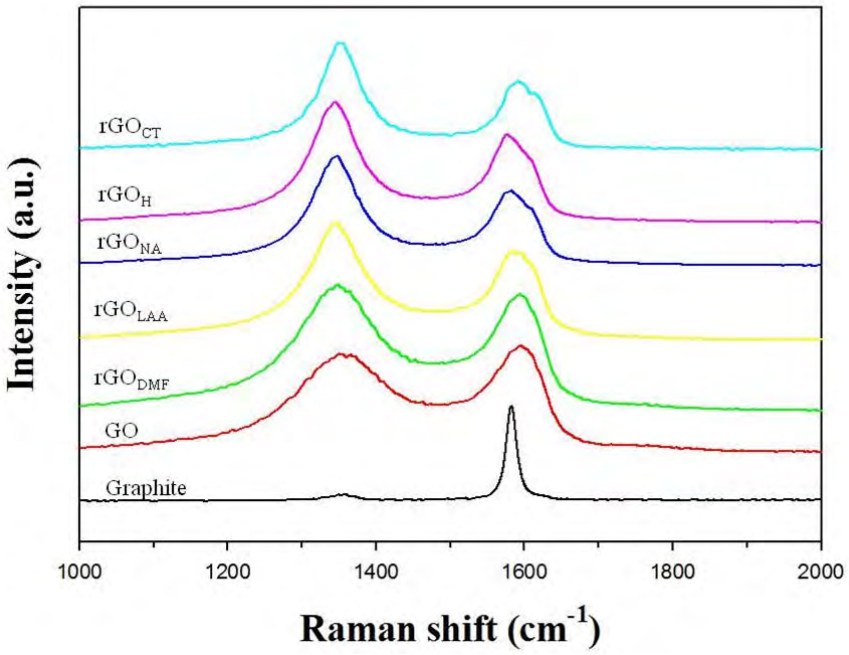

(a)

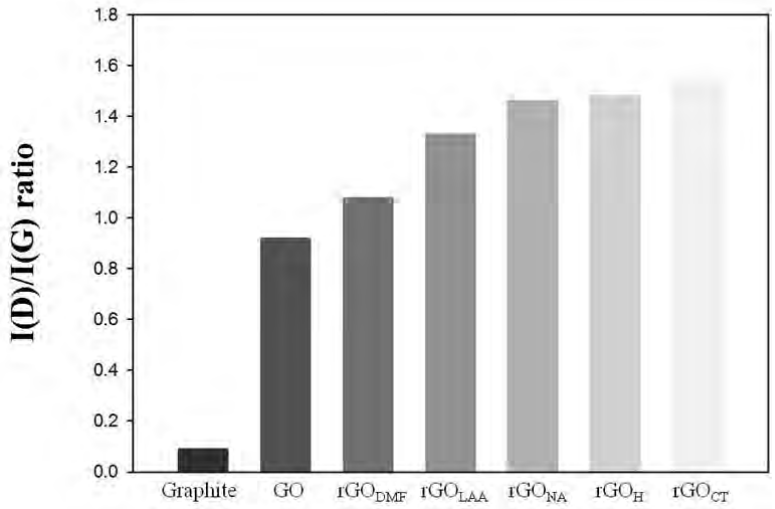

(b)

Figure 9. (a) Raman spectra and (b) their I(D)/I(G) ratios of the rGO$_{CT}$, rGO$_{H}$, rGO$_{LAA}$, rGO$_{NA}$, and rGO$_{DMF}$. The two prominent peaks at ~ 1350 and ~1600 cm^{-1} correspond to the D and G bands, respectively.

3-2. Thermal reduction: Thermal reduction of the GO was studied in order to investigate the effect of the annealing temperature on the reduction of the GO. This study provided the basic information for the GO reduction in the GO/BBL composite which will be discussed in the other part of this report.

3-2-1. Removal of oxygen containing groups: Figure 10a shows TGA thermograms of the graphite and the GO powders in nitrogen atmosphere. Major weight loss of the GOs (~ 24 %) occurred in the range of 180 to 220 ^{o}C with a maximum degradation rate at ~ 210 ^{o}C although the graphite did not show weight loss until 500 ^{o}C. Weight loss of the GO was due to pyrolysis of the labile oxygen-containing groups. However, weight loss continued after the greatest weight loss at ~ 210 ^{o}C with a small slope indicating that pyrolysis of the oxygen-containing groups continued. The initial mass loss was due to the absorbed water even though we dried samples in the vacuum oven. Figures 10b-c show the XPS survey spectra of the GOs and the O/C ratios at different annealing temperatures (T_as). Graphitic C 1s and O 1s were observed at 284.7 and 531 eV, respectively. The peak height of the O 1s decreased although that of C 1s remained relatively constant as T_a increased. The significant reduction of the O/C ratio (~0.4 to ~0.2) happened at ~ 220 ^{o}C which is similar to the temperature at which TGA results showed an abrupt change. Thus, the combination of TGA, and XPS results suggest that the major oxygen-containing groups (produced during oxidation of the graphite) were removed at ~ 220 ^{o}C but continual removing of the oxygen-containing groups happened afterward.

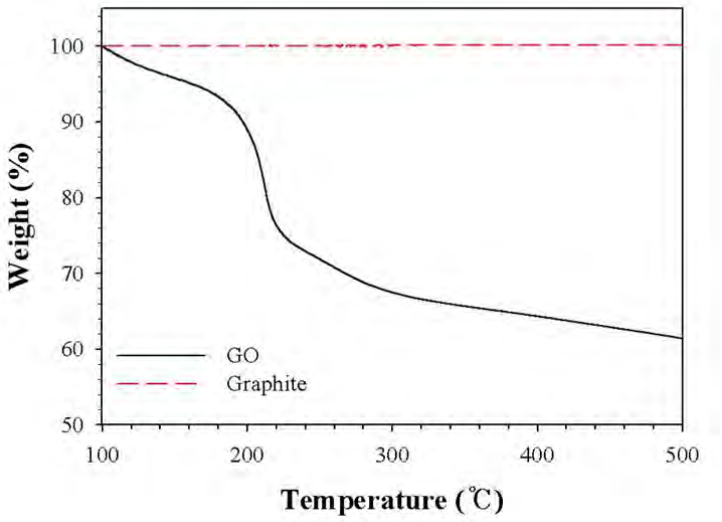
100
90
80
70
60
50
Weight (%)
GO
Graphite
100
200
300
400
500
Temperature (℃)

(a)

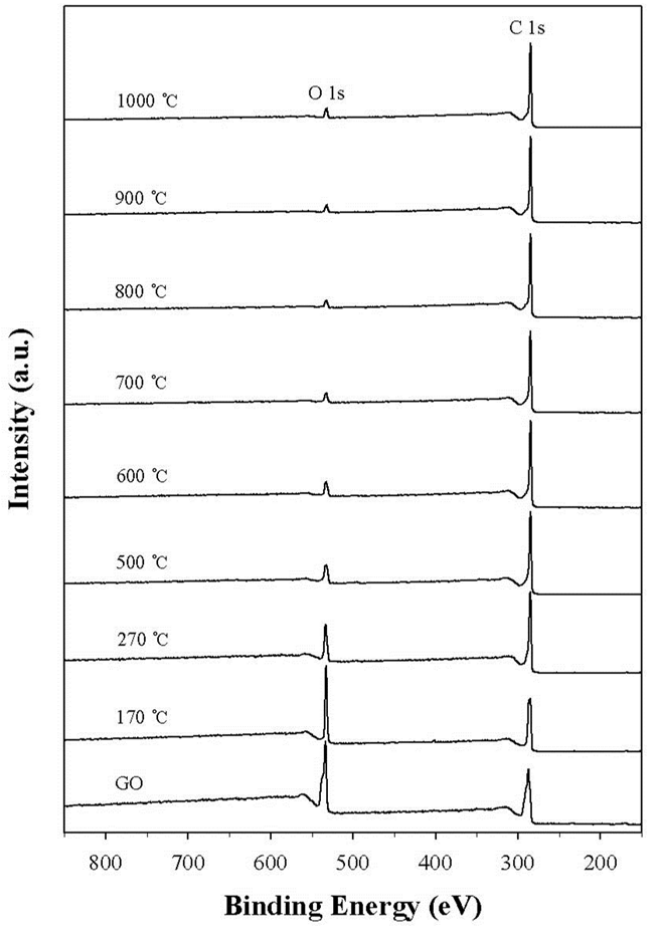
C 1s
O 1s
1000 ℃
900 ℃
800 ℃
700 ℃
600 ℃
500 ℃
270 ℃
170 ℃
GO
Intensity (a.u.)
800
700
600
500
400
300
200
Binding Energy (eV)

(b)

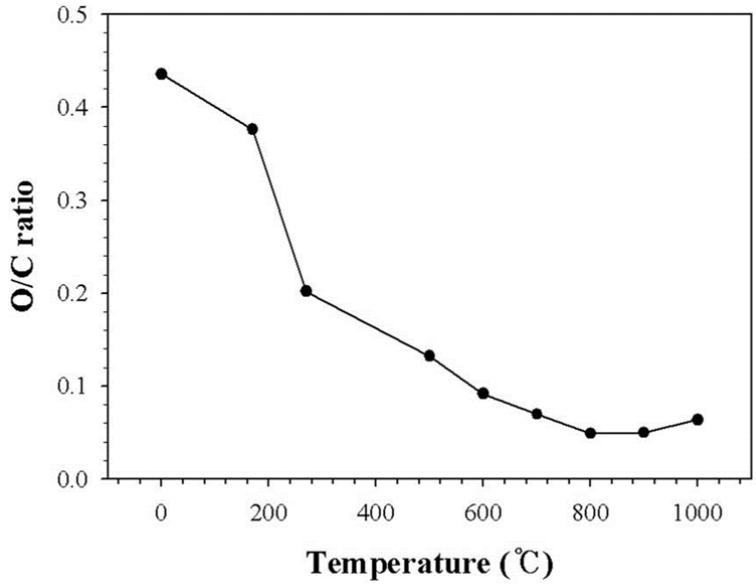

(c)

Figure 10. (a)TGA thermograms of the graphite and the graphite oxide in nitrogen atmosphere, (b) the XPS survey spectra of the graphite oxide films, and (c) the O/C ratios at different T_as.

3-2-2. X-ray analysis: Figures 11a-b show the two-dimensional X-ray diffraction patterns and their azimuthally averaged 2θ scans of the GO films annealed at different T_as for 1 hour when the X-ray beam was parallel to the film surface, respectively. Several peaks along the direction perpendicular to the film surface (the horizontal direction in Figure 11a) and the peak at $2\theta=43^o$ (d-spacing=2.1Å) along the direction parallel to the film surface (the vertical direction in Figure 11a) were observed. The peak positions of the horizontal peaks changed with T_a although the vertical positions did not. When the X-ray beam was perpendicular to the film surface, the isotropic rings were observed at the same d-spacings as those when the X-ray beam was parallel to the film surface. These different patterns depending on the X-ray beam direction were due to the planar orientation of the carbon layers of the GO film.

The unit cell dimensions of the graphite were $a = b = 2.456$ Å, $c = 6.694$ Å, and $\gamma = 120^o$ with hexagonal symmetry; the *a* and *b* axes are in the carbon layer, the *c* axis is perpendicular to it, and the *c* dimension is twice the distance between the adjacent carbon layers. The individual carbon layers were parallel to the surface of the GO film so that the horizontal peaks represent *00l* reflections and the vertical peak does an *hk0* in-plane reflection of the GO. The d-spacing of the vertical in-plane *hk0* peak is the same as that of the *100* reflection of the graphite indicating that the oxidation of the graphite and the annealing of the GO film did not change the basic hexagonal carbon network structure of the graphite although defects in the sheet could be formed during oxidation and thermal annealing. The positions of the horizontal peaks were strongly dependent on T_a as shown in Figure 11b. The X-ray pattern of the GO film at T_a=120 ^{o}C shows nearly the same pattern as that of the un-annealed GO film. However, the position of the main peak at $2\theta = 12.2^o$ (d-spacing=7.3 Å) shifted to the high 2θ angle (the decreased d-spacing) of $2\theta = 13.9^o$ (d-spacing=6.4 Å) at T_a=170 ^{o}C due to the removal of the oxygen-containing groups. The 170 ^{o}C is close to the temperature at which weight loss started in the TGA thermogram. The X-ray pattern at T_a = 220 ^{o}C shows the three peaks at $2\theta = 19.0^o$ (d-spacing = 4.7 Å), 23.5^o (d-spacing = 3.8 Å, the strongest one), and 26.4^o (d-spacing = 3.4 Å); the 220 ^{o}C is close to the temperature at which the rate of the degradation was maximum in the TGA thermogram. The peaks at T_a = 220 ^{o}C shifted to higher angles and became broader than that at T_a=170 ^{o}C due to further removal of the oxygen-containing groups and decrease of crystal size through cleavage of a stack of the carbon layers into small pieces. The d-spacings of these peaks were not multiple proportions indicating that three phases existed depending on the gap distance because only *00l* reflections with multiple proportions could appear in the horizontal direction if they came from one phase of the GO. Three phases were denoted as the phases I, II, and III

representing the observed 2θ angles starting from low to high, respectively and seemed to continue to exist in the range of T_a = 120 to 600 ^oC. Figure 11c shows the d-spacings of the three phases with respect to T_a. The peak position of the phase III did not change with T_a and is close to the *002* reflection of the graphite. This result suggests that the structure of the phase III may represent the graphite without the oxygen-containing functional groups. The peaks of the phases I and II continuously shifted to high angles and were eventually merged into that of the phase III after 700 ^oC. The width of the merged peak was getting broader as the T_a further increased indicating that the number of the stack of the intercalated carbon layers was getting diminished as T_a increased. The appearance of three different phases might be due to the inhomogeneous distribution of the oxygen-containing functional groups on the GO carbon layer. During the annealing, some oxygen-containing groups were more labile than the others. The gallery gap became narrow first in a certain part of the GO containing more labile oxygen-containing groups and eventually the same as that of the graphite by complete removal of the oxygen-containing groups with further heating at higher temperatures. From the X-ray analysis with the GO films annealed at different T_as, the dramatic change of the X-ray patterns was found at ~ 220 ^oC which is close to the temperature at which major weight loss and large reduction of the oxygen-containing groups occurred in the TGA thermogram and XPS survey spectra, respectively. In order to clarify what kind of oxygen-containing groups were removed at the individual T_as, the FT-IR measurement was performed.

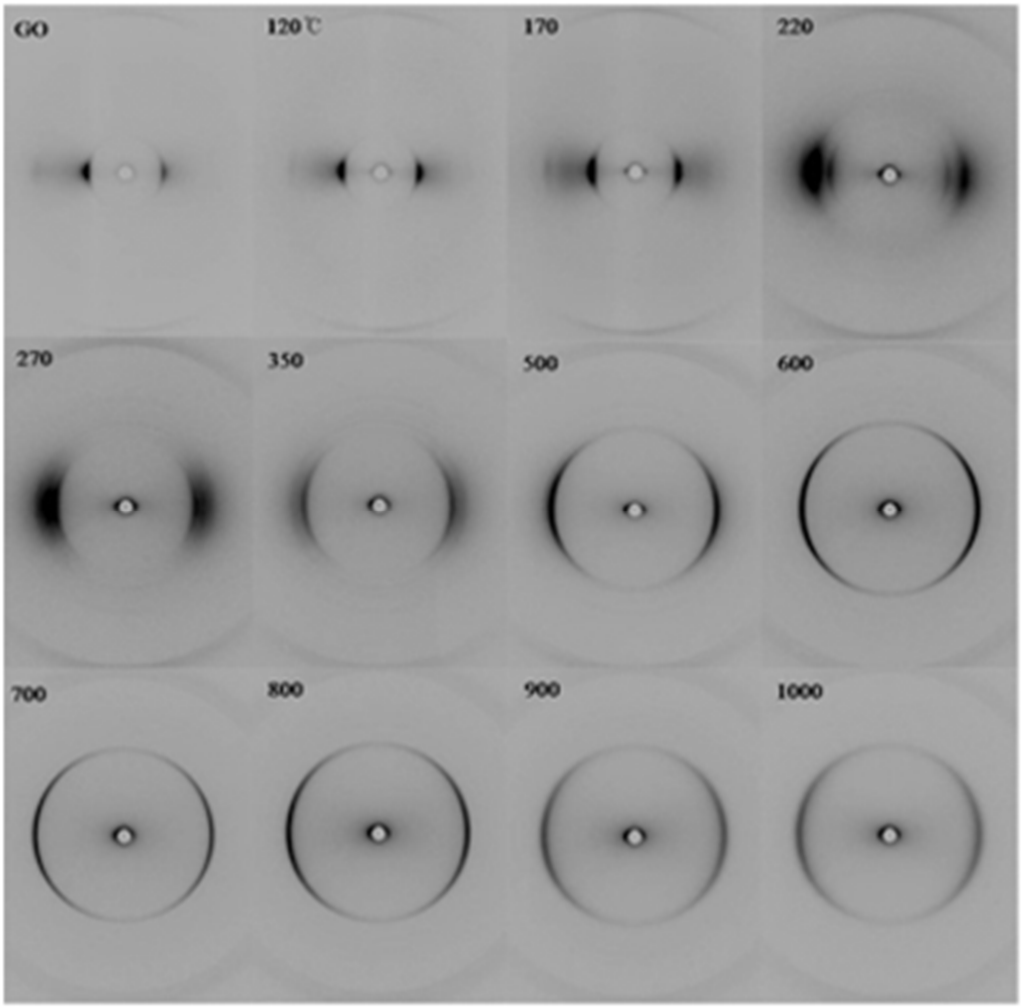

(a)

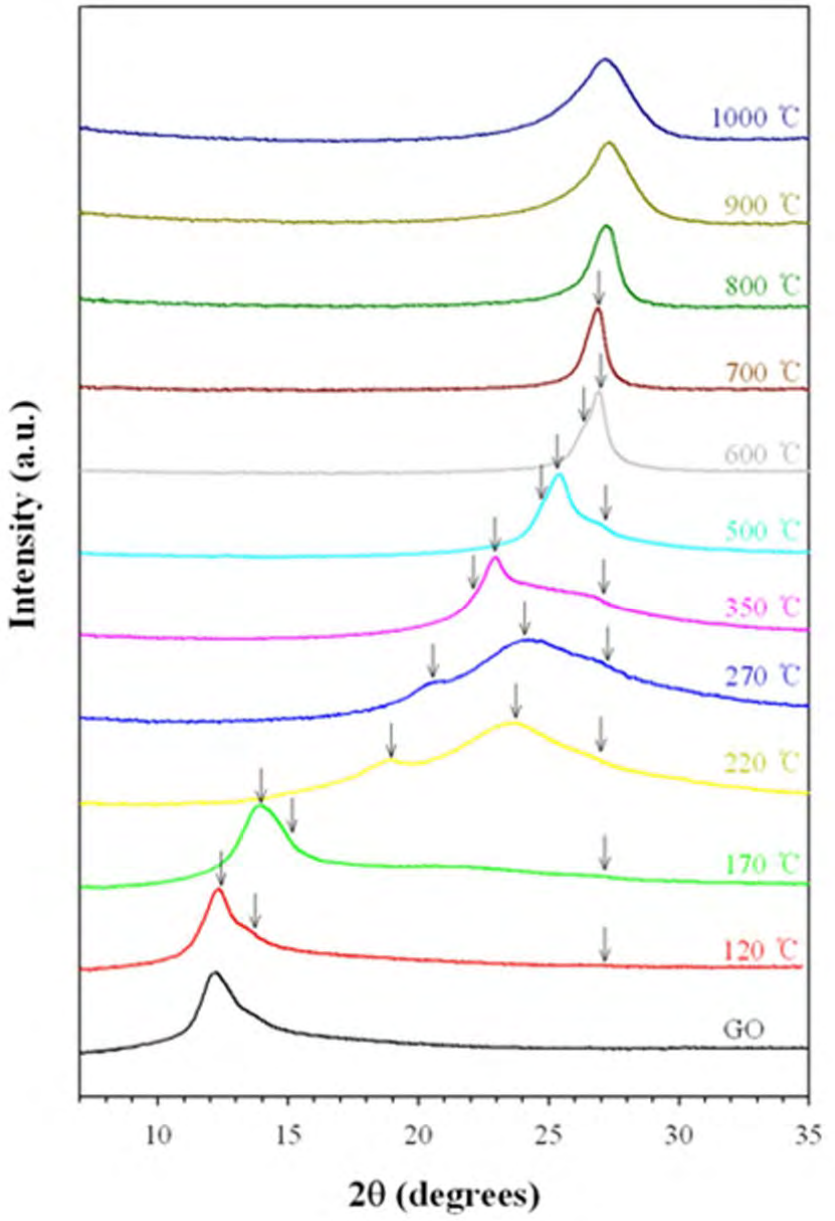
1000 ℃
900 ℃
800 ℃
700 ℃
600 ℃
500 ℃
350 ℃
270 ℃
220 ℃
170 ℃
120 ℃
GO
Intensity (a.u.)
10
15
20
25
30
35
2θ (degrees)

(b)

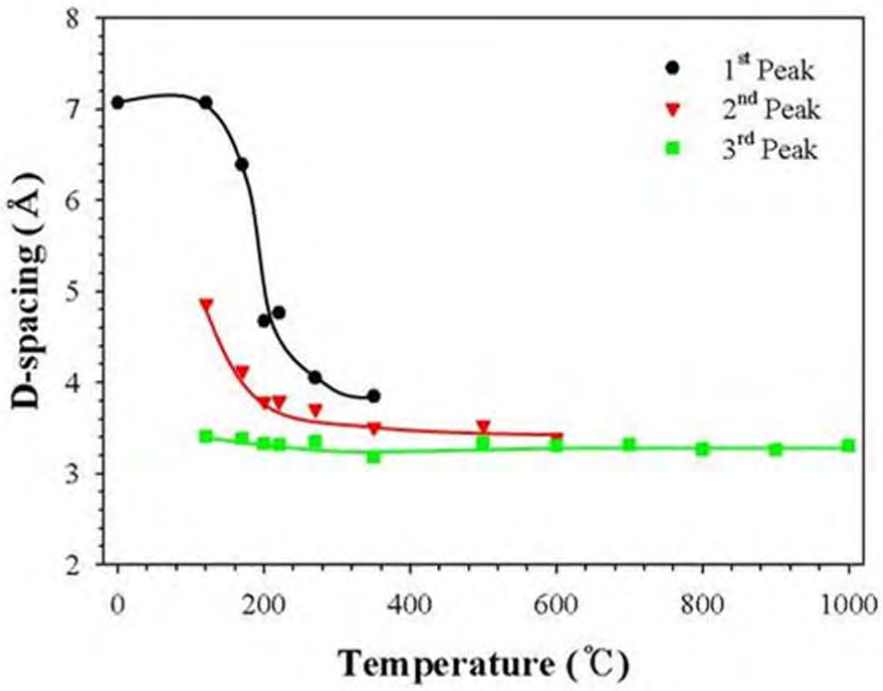

(c)

Figure 11. (a) The two dimensional X-ray diffraction patterns, (b) their azimuthally averaged 2θ scans of the graphite oxide films, and (c) the d-spacings of the observed reflections shown by arrows in (b); X-ray beam was parallel to the film surface after annealing the graphite oxide films at different T_as for 1 hour.

3-2-3. FT-IR and Raman spectroscopy: Figure 12a shows the IR spectra of the GO powders at different T_as. The IR spectrum of the GO without annealing represents the C=O stretching vibration at 1735 cm^{-1}, the C-O stretching vibration at 1050 cm^{-1}, –OH stretching vibration at 3400 cm^{-1}, O-H bending vibration in carboxylic group at 1420cm^{-1}, the stretching vibration of the epoxide moiety at 1220cm^{-1}, and the peak at 1620 cm^{-1} is due to the C=C stretching frequencies of aromatic skeleton or alkene groups of GO. After 170 ^{o}C, the peaks of the –OH stretching vibration at 3400 cm^{-1}, the O-H bending vibration in carboxylic group

at 1420cm^{-1}, and the C–O stretching vibration of the carboxylic group at 1050 cm^{-1} decreased as T_a increased and became the same level of the graphite (small traces) indicating that –OH and –COOH groups were removed. The stretching vibration of the epoxide moiety at 1220 cm^{-1} decreased gradually after 220 ^{o}C, and lasted until 1000 ^{o}C. The peak position of the C=C stretching continuously shifted from 1620 cm^{-1} to 1550 cm^{-1} until 220 ^{o}C and did not change after that probably due to the decrease of the defects in the carbon layer. The FT-IR spectra at $T_a \geq 700$ ^{o}C were almost the same as that of the graphite indicating that the partial thermal reduction was possible by annealing the graphite at $T_a \geq 700$ ^{o}C although some defects in the carbon layer were expected and the further exfoliation was necessary to get the completely separated graphene sheets. Figure 12b shows the Raman spectra for as prepared GO and the GO films annealed at 350, 700, and 1000 ^{o}C, respectively. The two prominent peaks at ~ 1350 and ~ 1600 cm^{-1} correspond to the D and G bands, respectively. It is evident from the D band of the annealed samples that sharpness and intensity increases with the increase in annealing temperatures which indicated the reduction of GO at higher annealing temperatures.

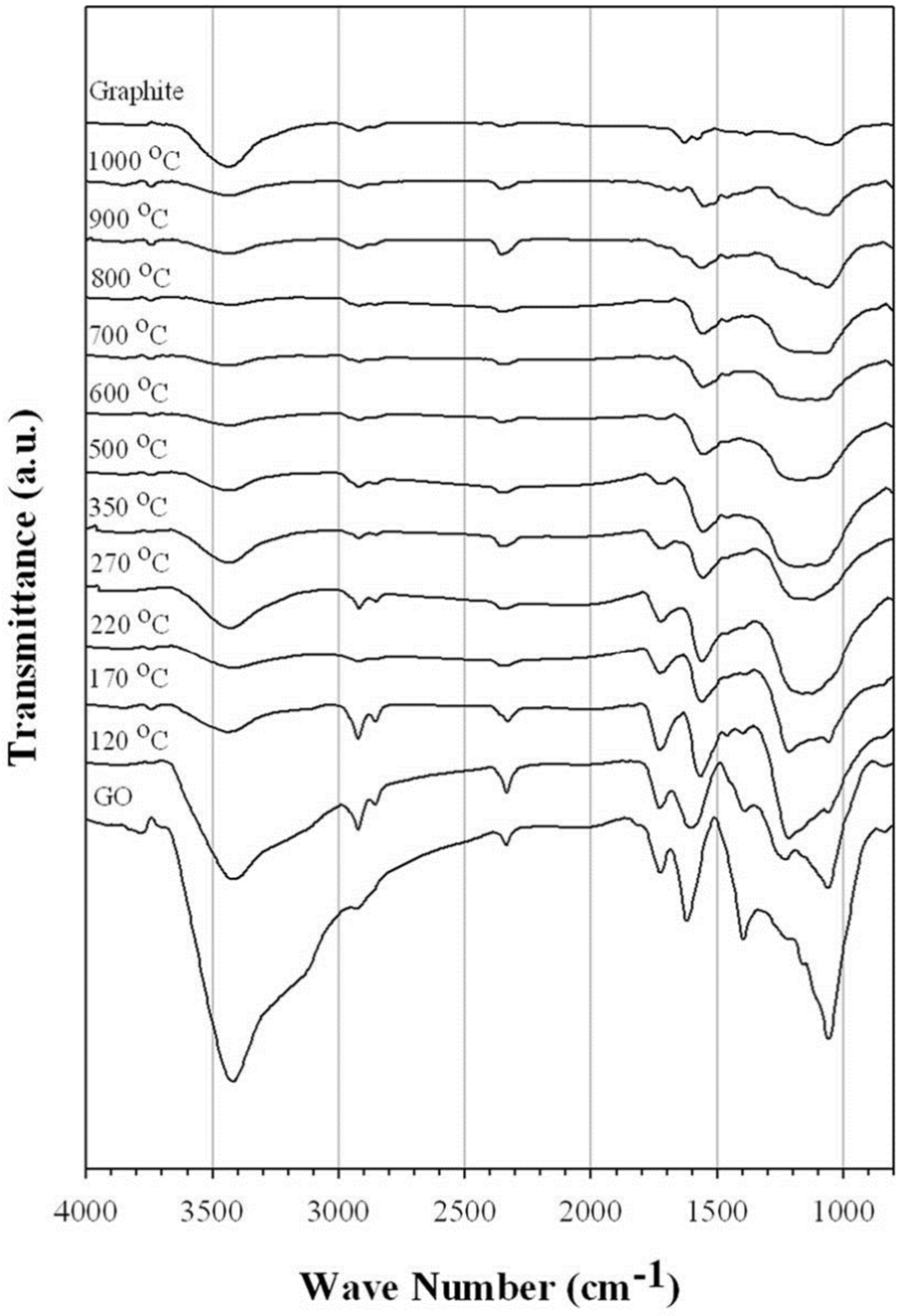
Graphite
1000 °C
900 °C
800 °C
700 °C
600 °C
500 °C
350 °C
270 °C
220 °C
170 °C
120 °C
GO
Transmittance (a.u.)
4000
3500
3000
2500
2000
1500
1000
Wave Number (cm-1)

(a)

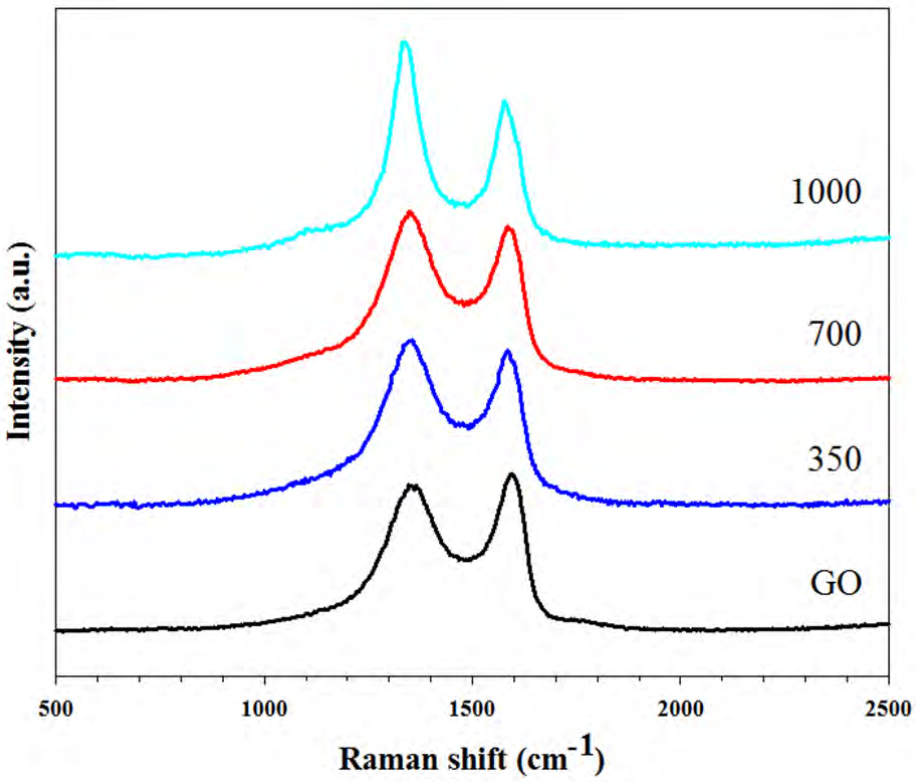

(b)

Figure 12. (a) IR spectra of the graphite oxides annealed at different T_as, (b) Evolution of the Raman spectra for as prepared GO and the GO films annealed at 350, 700, and 1000 ^{o}C, respectively. All of the spectra correspond to an exciting laser wavelength of 514.5 nm.

3-2-4. Electrical conductivity: Figure 13 shows the electrical conductivities of the GO films as functions of T_a and annealing time. The electrical conductivity of the GO film annealed at T_a=120 ^{o}C did not increase with annealing time. The electrical conductivity of the GO film annealed at T_a=170 ^{o}C slowly increased with annealing time although those at higher than 220 ^{o}C increased rapidly; the electrical conductivity of the GO film annealed at 220 ^{o}C increased to ~13 S/cm from below 10^{-6} S/cm (almost non-conducting) within 5 min while that annealed at 170 ^{o}C increased to ~2 S/cm within 20 min. The widely used reduction processes and thermal annealing at high temperatures enhance the electrical conductivity.

Although various reduction processes have been reported, high- electrical properties from GO remains a challenge due to the large number of structural defects and residual oxygen functional groups on the basal plane. The slight decrease in conductivity with time in Figure 13 might be due to the increase in space by removing some functional groups.

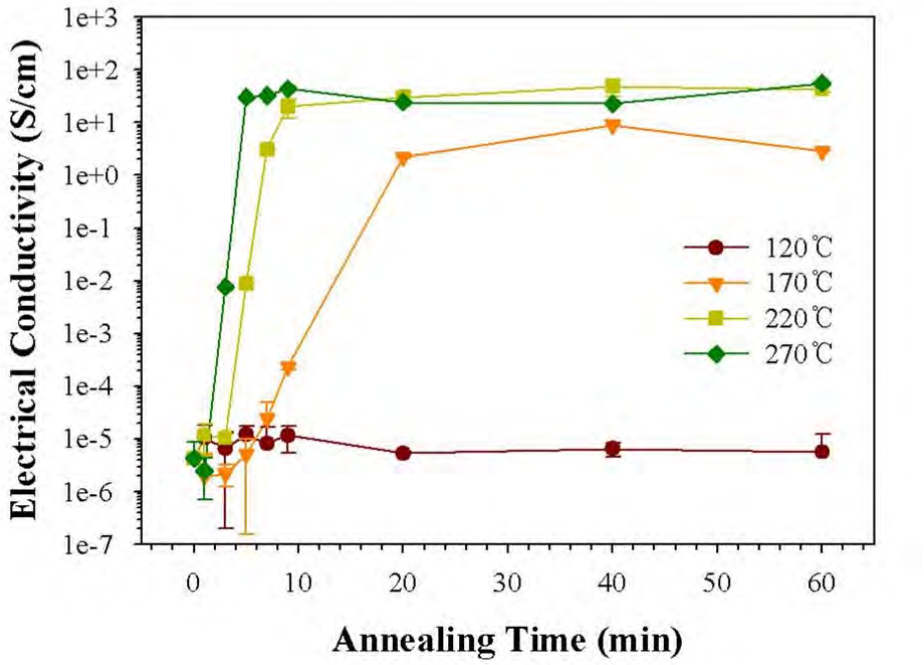

Figure 13. The change of the electrical conductivity of the graphite oxide films as functions of T_a and annealing time; the graphite oxide films were annealed under N_2 atmosphere.

Major weight loss and a sudden drop of the O/C ratio was found to occur at 220 ^{o}C from the TGA thermogram and XPS survey spectra, respectively so that the increase of the electrical conductivity during annealing might be a consequence of the gradual removal of the oxygen-containing groups which might lead to extension of the pi electron system. Thus, the thermal annealing at ~ 220 ^{o}C might be effective to partial recovery of the electrical conductivity from the almost non-conducting GO film although complete recovery might be possible with further annealing at high temperatures.

3-3. BBL/GO composite: The BBL/graphene nanocomposites were prepared with a solution blending in methanesulfonic acid (MSA) with GO, rGO_H, rGO_{NA}, rGO_{LAA}, rGO_{DMF}, and rGO_{CT}. Figure 14 shows the electrical conductivity vs. annealing temperature at different amounts of the GO (ϕs). Before annealing, the electrical conductivity increased as the ϕ increased. The conductivity continuously increased as the annealing temperature increased although the slope decreased after 270 °C. The conductivity levels of the annealed samples increased ~ 4 orders by annealing at 500 °C for 30 minutes; for example, 10^{-3} S/cm at ϕ = 90 wt% before annealing increased to 10 S/cm after annealing at 400°C. This increase might be due to partial reduction of the GO in the composite. It was found that most of the oxygen-containing functional groups in the GO were removed before 270 °C during the thermal annealing of the GO film. This high increase of the conductivity by annealing the BBL/GO films might be due to the thermal reduction of the GO in the BBL matrix.

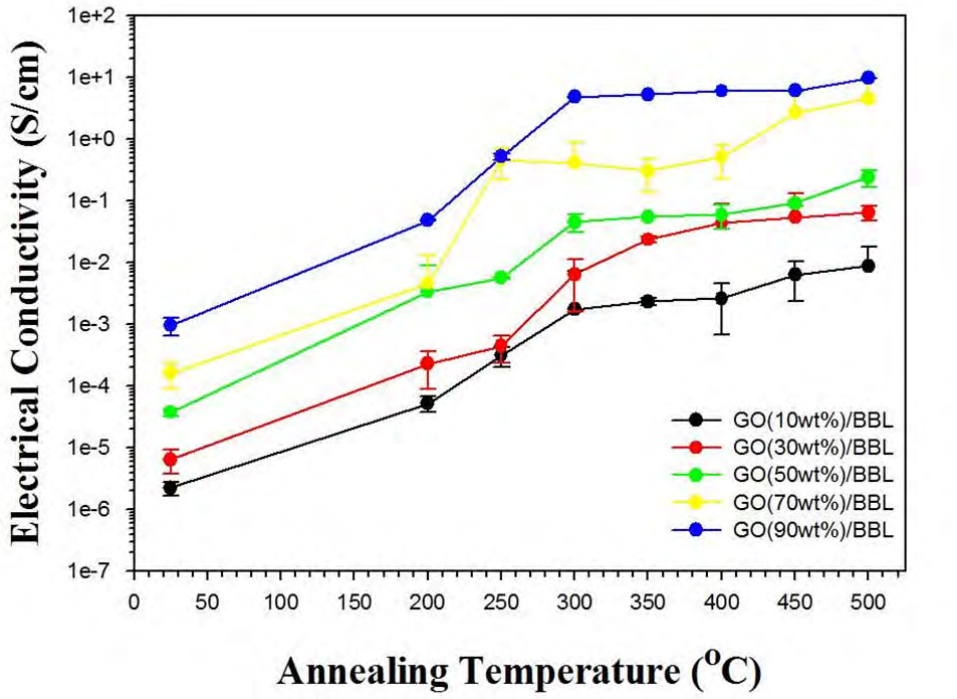

Figure 14. The electrical conductivity vs. annealing temperature at different ϕs; the annealing was done for 30 minutes at N_2 atmosphere.

Figure 15 shows the TGA thermogram of the GO(20 wt%)/BBL composites before and after annealing at 400 °C. The TGA thermogram of the GO(20 wt%)/BBL composites after annealing at 400 °C showed decomposition at ~380 to 480 °C with a ~ 2 wt% weight loss, little changed until 660 °C, and then decomposed after that. The TGA thermogram of the GO(20 wt%)/BBL composites before annealing showed several steps of the thermal decomposition until ~ 480 °C with a ~ 22 wt% weight loss, and then became similar to that after annealing at 400 °C. The weight loss until ~ 480 °C might be due to removal of the oxygen-containing groups in the GO because the BBL decomposed at ~ 700 °C. The oxygen-containing groups were already removed during annealing the composite film at 400

°C so that the weight loss of the annealed sample (~ 2 wt%) was small as compared to that of the un-annealed film (~ 22 wt%). This result also demonstrated that the thermal reduction was effective in the BBL/GO nanocomposite by annealing at relative low temperatures (< 400 °C).

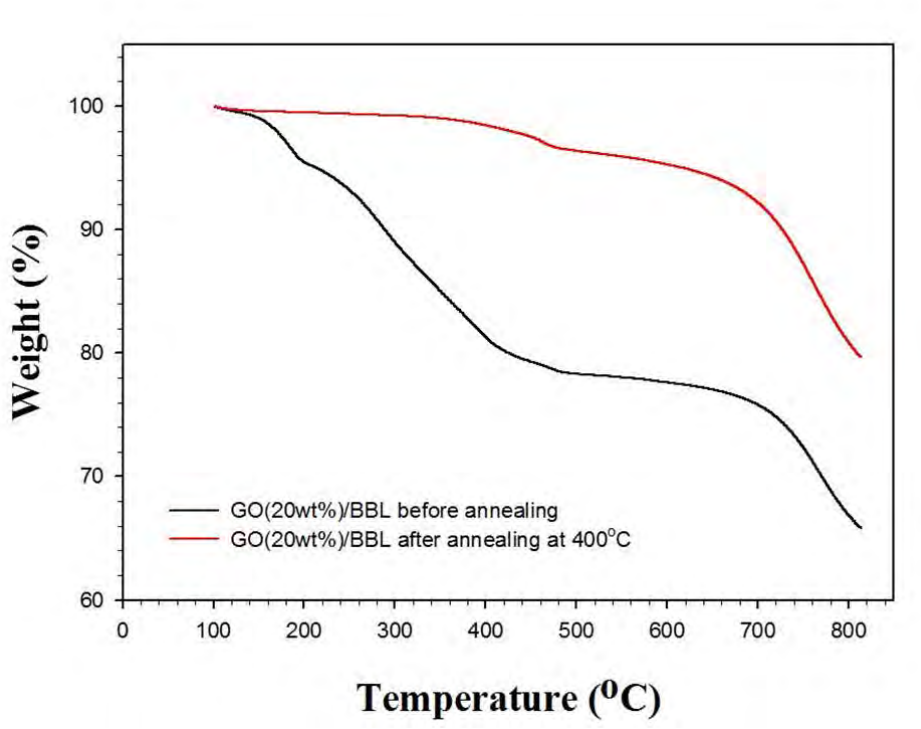

Figure 15. The TGA thermogram of the GO(20 wt%)/BBL composites before and after annealing at 400 °C.

Figure 16a shows the fractured surfaces of the the GO(10 wt%)/BBL nanocomposite film. The layered structure was observed. This layered structure might be due to the parallel orientation of the GO sheets with the nanocomposite film surface. Figure 16b exhibits its two-dimensional wide angle X-ray pattern. The normal of the film surface was parallel to the horizontal direction and the white curved line was due to the shadow of the film. The outer reflection showed stronger intensity in the meridian (vertical direction)

corresponding to the side-to-side interchain packing (100 plane) of 7.87 Å, whereas the inner reflection shows the stronger intensity in the equator (horizontal direction) corresponding to the face-to-face packing (010 plane) of 3.37 Å. This X-ray patterns can be interpreted that the (010) planes, where this plane is considered to be the large molecular plane, are lying perpendicular to the film surface plane with the chain axis (c-axis) being parallel to the film surface in a random manner. The results are exactly identical to the X-ray results of rigid-rod PBT film[81], suggesting the same growth mechanism of chain aggregation from the solution. Preferred growth in the direction of π-π interaction, as suggested by Roche[82] for the PBT film, would probably result in **such a unusual anisotropic micro-structure in** the BBL film. In addition to the reflections of the BBL crystal, the scattering along the equator (horizontal direction) originating from the beam stopper was observed. This scattering was due to the GO sheets which were oriented parallel to the BBL film. This result was consistent with the SEM micrograph of the fractured surface (Figure 16a) which showed the parallel orientation of the GO sheet with the composite film.

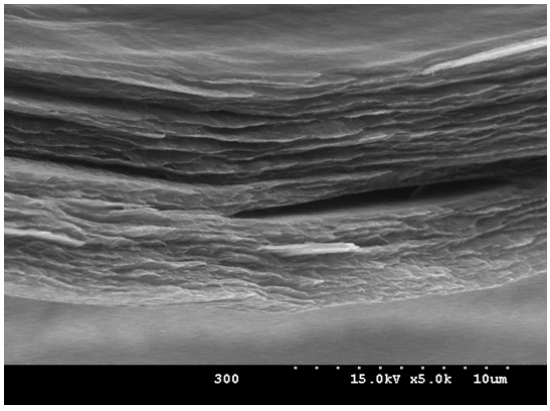

(a)

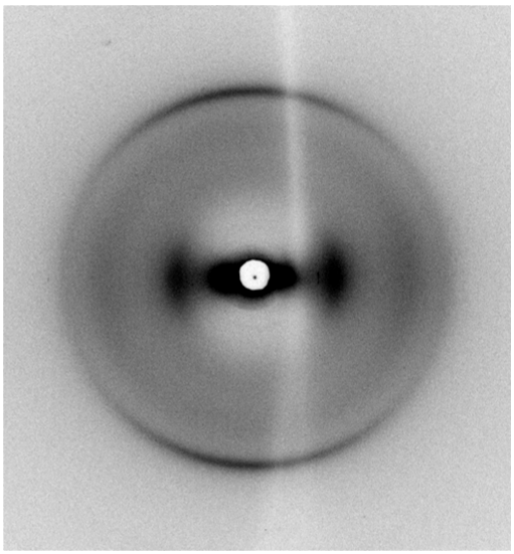

(b)

Figure 16. (a) The fractured surfaces of the the GO(10 wt%)/BBL nanocomposite and (b) its two-dimensional wide angle X-ray pattern; the normal of the film surface is parallel to the horizontal direction; the white curved line was due to the shadow of the film .

3-3. BBL/rGO composite

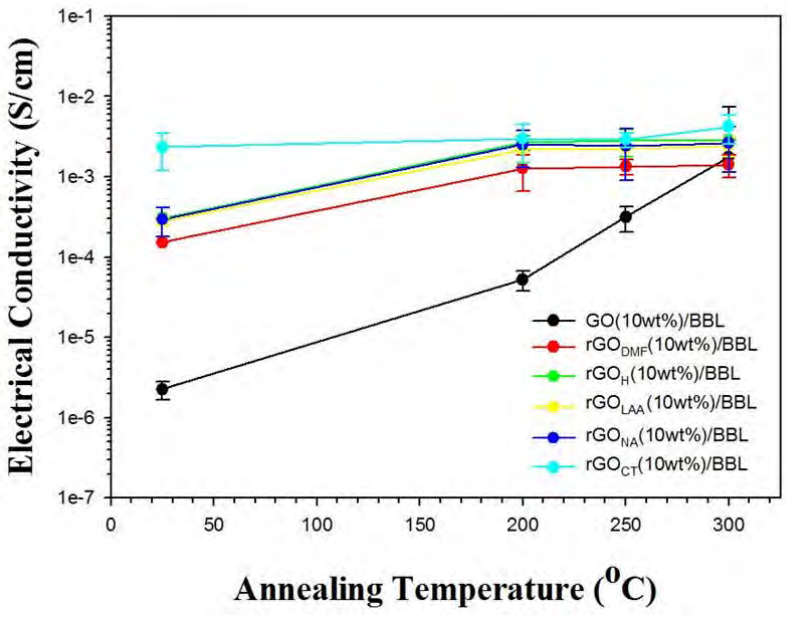

Figure 17. The electrical conductivity vs. annealing temperature of the rGO_H(10 wt%)/BBL, rGO_{LAA}(10 wt%)/BBL, rGO_{NA}(10 wt%)/BBL, and rGO_{DMF}(10 wt%)/BBL.

Figure 17 shows the electrical conductivity vs. annealing temperature of the rGO_H(10 wt%)/BBL, rGO_{LAA}(10 wt%)/BBL, rGO_{NA}(10 wt%)/BBL, and rGO_{DMF}(10 wt%)/BBL. The electrical conductivity of the rGO_{CT} (10 wt%)/BBL nanocomposite was ~ 0.0023 S/cm, and those of the rGO_H(10 wt%)/BBL, rGO_{LAA}(10 wt%)/BBL, rGO_{NA}(10 wt%)/BBL, and rGO_{DMF}(10 wt%)/BBL are 0.0003, 0.0003, 0.0003, 0.0002 S/cm, respectively. The electrical conductivity of the rGO_{CT} (10 wt%)/BBL nanocomposite is approximately one

order higher than those of other nanocomposites because the additional thermal reduction of GO was conducted to the already chemically-reduced GO by $NaBH_4$. This result indicates that the rGO_{CT} was well dispersed in the BBL although the more hydrophobic interactions between the rGO_{CT}s could be expected by combined thermal and chemical reductions. This good dispersion might be due to the interactions of the delocalized π elections in the BBL and the rGO_{CT}s. The rGO_{CT} (10 wt%)/BBL nanocomposite showed a small increase of the electrical conductivity from 0.002 to 0.004 S/cm by annealing at 300 °C for 30 minutes although the conductivities of the rGO_{NA}(10 wt%)/BBL, rGO_{H}(10 wt%)/BBL, rGO_{LAA}(10 wt%)/BBL increased from 0.0003±0.0001 to 0.003±0.001 S/cm by annealing at 300 °C for 30 minutes, almost one order increase, reaching to ~ that of rGO_{CT} (10 wt%)/BBL (0.004 S/cm). This increase of the conductivity might be due to the thermal reduction of the remained oxygen-containing groups of the rGO in the composite by annealing at a relatively low temperature (300 °C).

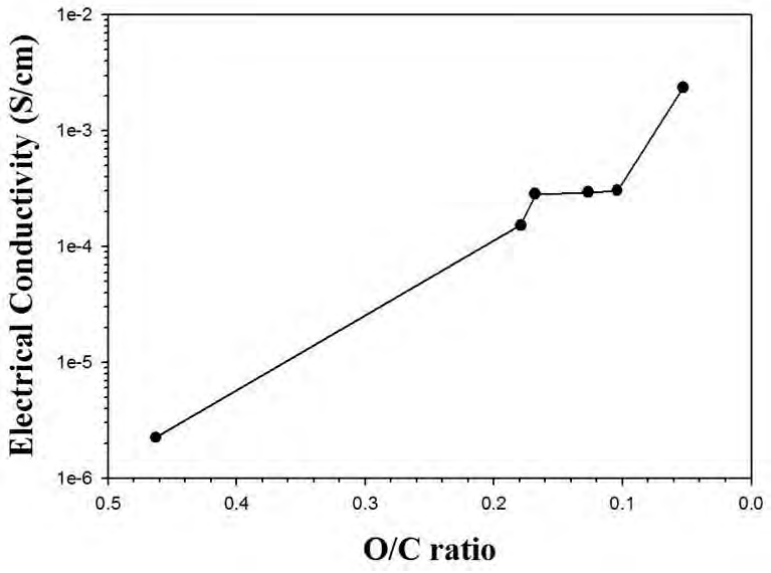

Figure 18. The electrical conductivity of the rGO_{H}(10 wt%)/BBL, rGO_{LAA}(10 wt%)/BBL, rGO_{NA}(10 wt%)/BBL, and rGO_{DMF}(10 wt%)/BBL vs. O/C ratios of rGOs.

Figure 18 shows the electrical conductivity of the the rGO_H(10 wt%)/BBL, rGO_{LAA}(10 wt%)/BBL, rGO_{NA}(10 wt%)/BBL, and rGO_{DMF}(10 wt%)/BBL vs. O/C ratios of rGOs. The electrical conductivity of the nanocomosite increased as the O/C ratio of the added rGO increased indicating that the quality of the filler determined the electrical conductivity of the composite. The electrical conductivity of the nanocomposite is strongly dependent on the electrical conductivity and dispersion of the filler. If the dispersion of the filler was not good in the polymer matrix, high electrical conductivity of the composite might not be expected even with the filler having high electrical conductivity. Thus, this result strongly indicates that the rGOs were well dispersed in the BBL matrix due to the interactions between the delocalized π electrons in BBL and rGOs.

4. Conclusion: The graphene oxides (GOs) and reduced GOs (rGOs) were well dispersed in BBL due to the interactions between the delocalized π electrons in both BBL and the carbon sheets of the graphene so that the electrical-conductivity levels of the composites were proportional to those of the rGOs. The thermal reduction after dispersing GOs in BBL was also possible due to the high thermal degradation temperature of BBL (> 600 °C). The electrical conductivity of the GO/BBL composite increased ~ 4 orders by annealing at 500 °C for 30 minutes. Thus, we found that the chemically-reduced GOs was applicable to the rGO/BBL nanocomposite system and the post-heat treatment of the GO/BBL composite was also effective to impart good electrical conductivity to BBL.

5. References

1. (a) K. S. Novoselov, A. K. Geim, S. V. Morozov, D. Jiang, M. I. Katsnelson, I. V.

Grigorieva, S. V. Dubonos, and A. A. Firsov, *Nature London* **2005**, 438, 197. (b) K. S. Novoselov, A. K. Geim, S. V. Morozov, D. Jiang, Y. Zhang, S. V. Dubonos, I. V. Grigorieva, and A. A. Firsov, *Science* **2004**, 306, 666. (c) S. Stankovich, D. A. Dikin, G. H. B. Dommett, K. M. Kohlhaas, E. J. Zimney, E. A. Stach, R. D. Piner, S. T. Nguyen, and R. S. Ruoff, *Nature London* **2006**, 442, 282.

2. Geim, A. K.; Novoselov, K. S. *Nat. Mater.* **2007**, 6(3), 183.

3. Kopelevich, Y.; Esquinazi, P. *Adv. Mater.* **2007**, 19, 4559.

4. Zhang, Y. B.; Tan, Y. W.; Stormer, H. L.; Kim, P. *Nature* **2005**, 438, 201.

5. M. Y. Han, B. Oezyilmaz, Y. Zhang, P. Kim, *Phys. Rev. Lett.* **2007**, 98, 206805.

6. (a) K. S. Novoselov, A. K. Geim, S. V. Morozov, D. Jiang, M. I. Katsnelson, I. V. Grigorieva, S. V. Dubonos, and A. A. Firsov, *Nature, London* **2005**, 438, 197. (b) J. Nilsson, A. H. C. Neto, F. Guinea, and N. M. R. Peres, *Phys. Rev. Lett.* **2006**, 97, 266801. (c) C. Gomez-Navarro, R. T. Weitz, A. M. Bittner, M. Scolari, A. Mews, M. Burghard, and K. Kern, *Nano Lett.* **2007**, 7, 3499. (d) A. A. Balandin, S. Ghosh, W. Z. Bao, I. Calizo, D. Teweldebrhan, F. Miao, and C. N. Lau, *Nano Lett.* **2008**, 8, 902. (e) M. Poot and H. S. J. van der Zant, *Appl. Phys. Lett.* **2008**, 92, 063111. (f) H. M. Wang, Y. H. Wu, Z. H. Ni, and Z. X. Shen, *Appl. Phys. Lett.* **2008**, 92, 053504.

7. Ramanathan, T.; Abdala, A. A.; Stankovich, S.; Dikin, D. A.; Herrera-Alonso, M.; Piner, R. D.; Adamson, D. H.; Schniepp, H. C.; Chen, X.; Ruoff, R. S.; *et al*. *Nat. Nanotechnol.* **2008**, 3, 327.

8. Wang, X.; Zhi, L. J.; Mullen, K. *Nano Lett.* **2008**, 8, 323.

9. Eda, G.; Fanchini, G.; Chhowalla, M. *Nat. Nanotechnol.* **2008**, 3, 270.

10. Yoo, E.; Kim, J.; Hosono, E.; Zhou, H.; Kudo, T.; Honma, I. *Nano Lett.* **2008**, 8, 2277.

11. Vivekchand, S. R. C.; Rout, C. S.; Subrahmanyam, K. S.; Govindaraj, A.; Rao, C. N. R. *J.*

Chem. Sci. **2008**, 120, 9.

12. Liu, Q.; Liu, Z. F.; Zhang, X. Y.; Zhang, N.; Yang, L. Y.; Yin, S. G.; Chen, Y. S. *Appl. Phys. Lett.* **2008**, 92, 223303.

13. Wang, X.; Zhi, L. J.; Tsao, N.; Tomovic, Z.; Li, J. L.; Mullen, K. *Angew. Chem., Int. Ed.* **2008**, 47, 2990.

14. Wu, Z. S.; Pei, S.; Ren, W.; Tang, D.; Gao, L.; Liu, B.; Li, F.; Liu, C.; Cheng, H. M. *Adv. Mater*. **2008**, DOI: 10.1002/adma200802560.

15. Mori, T.; Kikuzawa, Y.; Takeuchi, H. *Org. Electron.* **2008**, 9, 328.

16. Schedin, F.; Geim, A. K.; Morozov, S. V.; Hill, E. W.; Blake, P.; Katsnelson, M. I.; Novoselov, K. S. *Nat. Mater.* **2007**, 6, 652.

17. Dresselhaus, M. S. & Dresselhaus, G. *Adv. Phys.* **2002**, 51, 1.

18. Hirata, M., Gotou, T., Horiuchi, S., Fujiwara, M. & Ohba, M. *Carbon* **2004**, 42, 2929.

19. Yu, M. F., Lourie, O., Moloni, K., Kelly, T. F. & Ruoff, R. S. *Science* **2000**, 287, 637.

20. *J. Mater. Sci*. **2008**, 43, 5092.

21. Chung, D. D. L. *J. Mater. Sci.* **2004**, 39, 2645.

22. Stankovich, S. et al. *J. Mater. Chem.* **2006**, 16, 155.

23. Berger, C.; Song, Z. M.; Li, X. B.; Wu, X. S.; Brown, N.; Naud, C.; Mayo, D.; Li, T. B.; Hass, J.; Marchenkov, A. N.; *et al. Science* **2006**, 312, 1191.

24. Sutter, P. W.; Flege, J. I.; Sutter, E. A. *Nat. Mater.* **2008**, 7, 406.

25. Stankovich, S.; Dikin, D. A.; Piner, R. D.; Kohlhaas, K. A.; Kleinhammes, A.; Jia, Y.; Wu, Y.; Nguyen, S. T.; Ruoff, R. S. *Carbon* **2007**, 45, 1558.

26. Stankovich, S.; Piner, R. D.; Nguyen, S. T.; Ruoff, R. S. *Carbon* **2006**, 44, 3342.

27. Li, D.; Muller, M. B.; Gilje, S.; Kaner, R. B.; Wallace, G. G. *Nat. Nanotechnol.* **2008**, 3, 101.

28. (a) Stankovich S, Dikin DA, Piner RD, Kohlhaas KM, Kleinhammes A, Jia Y, et al. *Carbon* **2007**, 45(7), 1558. (b) Stankovich S, Dikin DA, Dommett GHB, Kohlhaas KM, Zimney EJ, Stach EA, et al. *Nature* **2006**, 442(7100), 282.

29. Szabo, T.; Berkesi, O.; Forgo, P.; Josepovits, K.; Sanakis, Y.; Petridis, D.; Dekany, I. *Chem. Mater.* **2006**, 18, 2740.

30. Hirata, M., Gotou, T. & Ohba, M. *Carbon* **2005**, 43, 503.

31. Szabo, T., Szeri, A. & Dekany, I. *Carbon* **2005**, 43, 87.

32. J. I. Paredes, S. Villar-Rodil, A. Martinez-Alonso, J. M. D. Tascon, *Langmuir* **2008**, 24, 10560

33. Kovtyukhova, N. I. et al. *Chem. Mater.* **1999**, 11, 771.

34. Kotov, N. A., Dekany, I. & Fendler, J. H. *Adv. Mater.* **1996**, 8, 637.

35. Cassagneau, T., Guerin, F. & Fendler, J. H. *Langmuir* **2000**, 16, 7318.

36. Gomez-Navarro, C.; Weitz, R. T.; Bittner, A. M.; Scolari, M.; Mews, A.; Burghard, M.; Kern, K. *Nano Lett.* **2007**, 7, 3499.

37. Becerril, H. A.; Mao, J.; Liu, Z.; Stoltenberg, R. M.; Bao, Z.; Chen, Y. *ACS Nano* **2008**, 2, 463.

38. (a) S. Stankovich, R. D. Piner, X. Q. Chen, N. Q. Wu, S. T. Nguyen, R. S. Ruoff, J. Mater. Chem. **2006**, 16, 155.; (b) S. Stankovich, D. A. Dikin, R. D. Piner, K. A. Kohlhaas, A. Kleinhammes, Y. Jia, Y. Wu, S. T. Nguyen, R. S. Ruoff, *Carbon* **2007**, 45, 1558.

39. Kim, U. J.; Liu, X. M.; Furtado, C. A.; Chen, G.; Saito, R.; Jiang, J.; Dresselhaus, M. S.; Eklund, P. C. *Phys. Rev. Lett.* **2005**, 95, 157402/1.

40. Donner, S.; Li, H. W.; Yeung, E. S.; Porter, M. D. *Anal. Chem.* **2006**, 78, 2816.

41. Schniepp, H. C.; Li, J. L.; McAllister, M. J.; Sai, H.; Herrera-Alonso, M.; Adamson, D. H.; Prud'homme, R. K.; Car, R.; Saville, D. A.; Aksay, I. A. *J. Phys.Chem. B* **2006**, 110, 8535.

42. McAllister, M. J.; LiO, J. L.; Adamson, D. H.; Schniepp, H. C.; Abdala, A. A.; Liu, J.; Herrera-Alonso, M.; Milius, D. L.; CarO, R.; Prud'homme, R. K.; *et al*., *Chem. Mater.* **2007**, 19, 4396.

43. Wang CS, Lee CY-C, Arnold FE. *Mater.Res.Soc.Symp.Proc.* **1992**, 247, 747.

44. Agrawal AK, Wang CS, Song HH. *Mater.Res.Soc.Symp.Proc.* **1994**, 328, 279

45. Narayan KS, Alagiriswamy AA, Spry R. *J. Physical Rreview B.* **1999**, 59(15), 10054.

46. Wilbourn K, Murray RW. *Macromolecules*. **1998**, 21, 89.

47. Yohannes T, Neugebauer H, Jenekhe SA, Sariciftci NS. *Synthetic Metals*. **2001**, 116, 241.

48. Yohannes T, Neugebauer H, Luzzati S, Catellani M, Jenekhe SA, Sariciftci NS. *J.Phys.Chem.B.* **2000**, 104, 9430.

49. Quinto M, Jenekhe SA, Bard A, *J. Chem.Mater*. **2001**, 13, 2824.

50. Narayan KS, Taylor BE, Spry RJ, Ferguson JB. *Journal of Luminescence* **1994**, 60&61, 482.

51. Narayan KS, Taylor BE, Spry RJ, Ferguson JB. *J. Appl. Phys*. **1995**, 77(8), 3938.

52. Antoniadis H, Abkowitz MA, Osaheni JA, Jenekhe SA, Stolka M. *Synthetic Metals*. **1993**, 60, 149.

53. Jenekhe SA, De Paor LR, Chen XL, Tarkka RM. *Chem. Mater.* **1996**, 8(10), 2401.

54. Lindle JR, Bartoli FJ, Hoffman CA, Kim O-K, Lee YS, Shirk JS, Kafafi ZH. *Appl. Phys. Lett.* **1990**, 56(8), 712.

55. Stolka M, Abkowitz MA, Ong BS, Jenekhe SA. *US Patent*. **1993**, 5, 248, 580.

56. Osaheni JA, Jenekhe SA, Peristein *J. J. Phys. Chem*. **1994**, 98, 12727.

57. Manoj AG, Alagiriswamy AA, Narayan KS, *J. Appl. Phys*. **2003**, 94(6), 4088.

58. Babel A, Jenekhe SA. *Adv. Mater.* **2002**, 14(5), 371.

59. Narayan KS, Manoj AG, Singh ThB, Alagiriswamy AA. *Thin Solid Films*. **2002**, 417, 75.

60. Manoj AG, Narayan KS. *Optical Materials*. **2002**, 21, 417.

61. Gowrishankar V, Luscombe CK, McGehee MD, Frechet JMJ. *Solar Energy Materials&Solar Cells*. **2007**, 91, 807.

62. (a) R.L. van Deusen, *J. Polym. Sci.*, Part B **1966,** 4, 211. R.L. van Deusen, O.K. Goins, A.J. Sicree, (b) *J. Polym. Sci.*, Part A-1 **1968**, 6, 1777. (c) F.E. Arnold, R.L. van Deusen, *Macromolecules* **1969**, 2, 497.

63. 1) (a) F. E. Arnold and R. L. Van Deusen, *Macromolecules* **1969,** 2, 497.; (b) F. E. Arnold and R. L. Van Deusen, *J. Appl. Polym. Sci*. **1971**, 15, 2035. 2) (a) S. A. Jenekhe, L. R. dePaor, X. L. Chen, and R. M. Tarkka, *Chem. Mater*. **1996**, 8, 2401. ; (b) C. S. Wang, C. Y. C. Lee, and F. E. Arnold, in *Electrical, Optical, and Magnetic Properties of Organic Solid State Materials*, edited by L. V. Chiang, A. F. Garito, and D. J. Sandman, No. 247 of MRS Symposia Proceedings ~Materials Research Society, Pittsburgh, **1992**, 747.

64. 1) (a) F. E. Arnold and R. L. Van Deusen, *Macromolecules* **1969**, 2, 497.; (b) F. E. Arnold and R. L. Van Deusen, *J. Appl. Polym. Sci*. **1971**, 15, 2035. 2) (a) S. A. Jenekhe, L. R. dePaor, X. L. Chen, and R. M. Tarkka, *Chem. Mater*. **1996**, 8, 2401.; (b) C. S. Wang, C. Y. C. Lee, and F. E. Arnold, in *Electrical, Optical, and Magnetic Properties of Organic Solid State Materials*, edited by L. V. Chiang, A. F. Garito, and D. J. Sandman, No. 247 of MRS Symposia Proceedings ~Materials Research Society, Pittsburgh, **1992**, 747. 3) (a) R. L. Van Deusen, *J. Polym. Sci., Polym. Lett.* Ed. **1966**, 4, 211.; (b) S. A. Jenekhe and S. J. Tibbetts, *J. Polym. Sci., Part B*: Polym. Phys. 1988, 26, 201.; (c) S. A. Jenekhe and P. O.Johnson, *Macromolecules* **1990**, 23, 4419.

65. L.R. Dalton, J. Thomson, H.S. Nalwa, *Polymer* **1987**, 28, 543.

66. J.H. Burroughes, D.D.C. Bradley, A.R. Brown, R.N. Marks, K. KacKay, R.H. Friend, P.L. Burns, A.B. Holmes, *Nature* **1990**, 347, 539. ; S.A. Jenekhe, M. Roberts, A.K. Agrawal, J.S.

Meth, H. Vanherzeele, *Mat. Res. Soc. Symp. Proc.* **1991**, 214.

67. *Solid-state Sci,* **1985**, 63, 2.

68. J. W. Blatchford and A. J. Epstein, *Am. J. Phys.* **1996**, 64, 120.

69. (a) 0. K. Kim, *J. Polym. Sci.: Polym. Lett.* **1982**, 20, 662.; (b) *Mol. Cryst. Liq. Cryst.* **1984**, 105, 161. ; S. A. Jenekhe, *ACS Polym. Mat. Sci Eng.* **1989**, 60, 419.

70. C. S. Wang, C. Y-C. Lee, and F. E. Arnold, in *ElectricalOptical, and Magnetic Properties of Organic Solid State Materials,* L. Y. Chiang, A. F. Garito, and D. J. Sandman, eds., *Mater. Res. SOCS. ymp. Proc*., Vol. 247, Pittsburgh, PA, **1992,** 747.

71. F. Coter, Y. Belaish, D. Davidov, E. Ehrenfreund, M.R. McLean, H.S. Nalwa, *Synth. Met*. **1989**, 29, 471.

72. C.-Y. Wang, TRIP 1 (1993) 199 and references therein.

73. (a) C.-S. Wang, C.Y.-C. Lee, F.E. Arnold, *Mat. Res. Soc. Symp. Proc*. **1992**, 247, 747. (b) A.K. Agrawal, C.-S. Wang, H.H. Song, *Mat. Res. Soc. Symp. Proc.* **1994**, 328, 279. (c) K.S. Narayan, A.A. Alagiriswamy, *R.J. Spry, Phys. Rev. B* **1999**, 59, 10054.

74. Bryning MB, Islam MF, Kikkawa JM, Yodh AG. *Adv Mater* **2005**, 17(9), 1186.

75. Kelong A, Yanlan L, Lehui L, Xiaoli C and Lihua H, *J. Mater. Chem., **2011***, 21, 3365–3370

76. Jiali Zhang, Haijun Yang, Guangxia Shen, Ping Cheng, Jingyan Zhang and Shouwu Guo, *Chem. Commun*. **2010**, 46, 1112–1114

77. Wei Gao, Lawrence B. Alemany, Lijie Ci and Pulickel M. Ajayan, NATURE CHEMISTRY **2009**, 1, 404.

78. Sasha Stankovich , Dmitriy A. Dikin, Richard D. Piner, Kevin A. Kohlhaas, Alfred Kleinhammes, Yuanyuan Jia, Yue Wu, SonBinh T. Nguyen, Rodney S. Ruoff, *Carbon* **2007**, 45, 1558–1565.

79. Junfeng Li, Hong Lin, Zhilong Yang, Jianbao Li, *CARBON* **2011**, 4 9, 3024 –3030

80. Kudin, Konstantin N.; Ozbas, Bulent; Schniepp, Hannes C.; Prud'homme, Robert K.; Aksay, Ilhan A.; Car, Roberto. *Nano Lett*. **2008**, 8, 36.

81. H. H. Song and C.-S. Wang, *Polym. Commu*. **1994**, 34.

82. E. J. Roche, *MRS Symp. Proc.* **1989**, 134, 457